Protective effects of Mkl1/2 against lipodystrophy and muscle atrophy via PI3K/AKT-independent FoxO repression

Atsushi Kubo[*,1], Keisuke Hitachi[2], Ryutaro Shirakawa[3] and Toshihiko Ogura[1]

[1]Department of Developmental Neurobiology, Institute of Development, Aging and Cancer, Tohoku University, Sendai, Japan
[2]Division for Therapies against Intractable Diseases, Center for Medical Science, Fujita Health University, Toyoake, Japan
[3]Department of Molecular and Cellular Biology, Institute of Development, Aging and Cancer, Tohoku University, Sendai, Japan

[*]Corresponding author. Tel: +81 22 717 8596; E-mail: atsushi.kubo.c7@tohoku.ac.jp

ABSTRACT

FoxO transcription factors are involved in the pathogenesis of lipodystrophy and muscle atrophy. FoxO proteins are phosphorylated and inactivated by PI3K/AKT signaling, but little is known about FoxO repressors other than this pathway. Here we show that the Srf cofactors Mkl1 and Mkl2 directly repress FoxO transcriptional activity independently of the PI3K/AKT pathway. Loss of *Mkl1/2* leads to overactivation of FoxO, which impairs the maintenance of both white adipose tissue (WAT) and skeletal muscle. In WAT, activated FoxO suppresses *Pparγ* and severely impairs white adipogenesis. In myotubes, FoxO induces the expression of atrophy-related genes (atrogenes), which is suppressed by Mkl1 and Mkl2. Mkl1 expression is reduced at the onset of muscle atrophy *in vivo*. Exogenous supplementation of skeletal muscle Mkl1 expression suppresses atrogene expression and induces muscle hypertrophy. Finally, both Mkl2 nuclear localization and *Mkl1/2* expression are upregulated by exercise, suggesting that *Mkl1/2* are involved in the inhibitory effect of exercise on muscle atrophy. These findings indicate that Mkl1/2 act as PI3K/AKT signaling independent repressors of FoxO and are essential for adipose and muscle tissue homeostasis.

INTRODUCTION

FoxO proteins are involved in many aspects of life[1,2]. In lower organisms, FoxO activation has been reported to increase lifespan[3], but in mammals there is emerging evidence that excessive FoxO activation is more likely to induce cellular senescence or age-related diseases[4,5]. Since FoxO proteins are known to be phosphorylated and

inactivated by the PI3K/AKT pathway[6], excessive FoxO activation is often associated with reduced responsiveness to insulin signaling. Adipose tissue and skeletal muscle are tissues closely associated with insulin resistance.

Excessive activation of Foxo1 in white adipose tissue (WAT) affects systemic metabolism and is implicated in the development of diabetes[5]. In addition, subcutaneous fat mass decreases with age. Since subcutaneous fat is thought to have beneficial effects on systemic metabolism, some age-related metabolic dysfunction may also be due to a lack of subcutaneous fat[7]. WAT maintains its plasticity through differentiation of adipose progenitor and stem cells (APSCs), but the differentiation capacity of aged APSCs is reduced[7,8]. It has been reported that Foxo1 overactivation negatively regulates both the initiation of *Pparγ* expression and the transcriptional activity of Pparγ itself, thereby suppressing adipocyte differentiation[9-12].

Besides *Foxo1*, *Foxo3* and *Foxo4* have overlapping functions in skeletal muscle. Skeletal muscle atrophy can be caused by a variety of factors, including aging, fasting, denervation, cancer cachexia, and glucocorticoid treatment, all of which are closely related to the activation of FoxO proteins[13-16]. Activated Foxo1/3/4 promotes proteasomal proteolysis of muscle proteins by inducing the expression of atrophy-related genes (atrogenes), including skeletal muscle-specific E3 ubiquitin ligases (*atrogin-1* and *MuRF1*)[16,17]. Glucocorticoids and the glucocorticoid receptor (GR) are also known to be involved in skeletal muscle atrophy. Glucocorticoids activate FoxO by dephosphorylation and also increase their expression[13,18,19]. GR and FoxO synergistically induce some atrogenes[20].

In contrast, exercise induces muscle hypertrophy and is known to be an effective intervention against muscle wasting[21]. Increased insulin responsiveness due to exercise is thought to influence muscle hypertrophy and suppression of atrophy, but the exact mechanisms are not well understood. Exercise is known to upregulate the expression of *PGC-1α*[22,23]. Overexpression of *PGC-1α* has been reported to be protective against muscle wasting[24,25]. However, overexpression of *PGC-1α* induces increased Akt protein levels, resulting in increased Foxo3 phosphorylation[26]. Therefore, the inhibitory effect of *PGC-1α* overexpression on muscle atrophy may be mediated in part through the enhancement of the PI3K/Akt pathway.

Mkl1 and *Mkl2* play important roles in the cardiovascular system by acting as cofactors for *Srf*[27,28]. They are thought to have overlapping molecular functions. However, in contrast to *Mkl1* knockout mice, *Mkl2* knockout mice are embryonic lethal[29,30]. *Mkl1* and *Mkl2* are also known as mechanosensitive transcription factors. Their subcellular localization, i.e. whether they are activated or not, is also regulated by intracellular actin

dynamics[27,28]. G-actin and importin bind competitively in the region around the RPEL domain of Mkl1 and Mkl2. Once actin polymerization has occurred, such as that induced by mechanical stress, it leads to nuclear accumulation of Mkl1/2 through a decrease in G-actin binding.

The association with laminopathy is another distinguishing feature of *Mkl1/2*. Mutations in *Lmna*, an intermediate filament protein that forms the nuclear lamina, are known to cause a variety of inherited diseases, including premature aging, lipodystrophy, muscular dystrophy, and dilated cardiomyopathy (DCM)[31,32]. *Lmna* deficiency or *Lmna* N195K mutation is closely associated with DCM pathogenesis, and it has been reported that nuclear translocation of Mkl1 is severely suppressed in cells carrying these mutations[33]. Interestingly, excessive FoxO activation is observed in the myocardium of mice with DCM associated with *Lmna* deficiency, and this dysregulation of *FoxO* is thought to be involved in disease progression[34]. However, the mechanism of FoxO overactivation caused by *Lmna* deficiency is not well understood.

In this study, we show that the *Srf* cofactors Mkl1 and Mkl2 repress FoxO protein activity through direct protein-protein interactions and function to maintain WAT and skeletal muscle mass.

RESULTS

Mkl2 knockout mice show a decrease in both white adipose tissue and skeletal muscle mass

Mkl2 knockout mice of the C57BL/6 strain are embryonic lethal due to cardiovascular developmental abnormalities, including dysplasia of the sixth pharyngeal arch artery and ventricular septal defects[29,30]. To investigate the function of *Mkl2* in the adult, we generated *Mkl2* KO mice by heterosis using crosses between the ICR strain and the C57BL/6N strain. *Mkl2* KO mice were significantly lighter than wild-type mice of the same litter (Dunnett's test, male mice: $p=0.0023$, female mice: $p < 0.0001$) (Fig. 1a). Significant reductions in WAT were observed in the inguinal, epididymal, gonadal and mesenteric regions (Fig. 1b, c, e, Supplementary Fig. 1a, c, d), while there was little change in the weight of brown adipose tissue (Supplementary Fig. 1b).

Mkl2 knockout mice had decreased skeletal muscle weight in the gastrocnemius, tibialis anterior, soleus, plantaris, and extensor digitorum longus muscles (21-22 weeks old, female mice, Fig. 1d, f, Supplementary Fig. 2). Thus, the reduction in body weight of *Mkl2* KO mice was mainly due to a reduction in WAT and skeletal muscle mass (Fig. 1c-f, Supplementary Fig. 1-2).

Mkl1/2 represses Foxo1/3/4 transcriptional activity independent of the PI3K/AKT signaling pathway

The loss of both WAT and skeletal muscle seen in *Mkl2* KO mice was reminiscent of the phenotype caused by overactivation of FoxO. Among the FoxO transcription factors, *Foxo1* is a dominant regulator of adipocyte differentiation[12]. Therefore, we first investigated whether *Mkl2* deletion is associated with Foxo1 overactivation in inguinal WAT tissue. We extracted RNA from the inguinal WAT of *Mkl2* KO mice and their littermate wild-type mice and analyzed the gene expression profiles. The resulting list of differentially expressed genes was then analyzed using Ingenuity Pathway Analysis (upstream analysis) to predict changes in the activation or inactivation status of transcription factors in *Mkl2* KO mice (Fig. 1g, Supplementary Table 1). The transcriptional activity of Srf, a transcription factor that interacts with Mkl2, was inhibited in *Mkl2* KO mice (Fig. 1g). Higher on the list than Srf was Foxo1, which was predicted to be in an activated state in *Mkl2* KO mice. Although the expression levels of several Foxo1 target genes tended to increase, there was no change in *Foxo1* mRNA levels in the WAT of *Mkl2* KO mice (Supplementary Fig. 3), indicating that the transcriptional activity of Foxo1 is upregulated in the WAT of *Mkl2* KO mice. In addition to *Foxo1*, *Foxo3* and *Foxo4* are also involved in skeletal muscle function[16]. Therefore, we further investigated whether Mkl2 can repress the transcriptional activity of Foxo1, Foxo3 and Foxo4 using a luciferase reporter with a FoxO binding site. Mkl2 was found to repress the transcriptional activity of Foxo1, Foxo3 and Foxo4 (Fig. 1h). FoxO proteins are phosphorylated by AKT and then exported to the cytoplasm where they are inactivated. Therefore, inhibition of the PI3K/AKT pathway inhibits FoxO phosphorylation and promotes their activation by accumulating in the nucleus. Indeed, the transcriptional activity of Foxo1, Foxo3 and Foxo4 was further increased by treatment with LY294002, an inhibitor of PI3K (Fig. 1i). Interestingly, even when the PI3K/AKT pathway was inhibited, Mkl2 repressed the transcriptional activity of Foxo1, Foxo3, and Foxo4 (Fig. 1i). A similar inhibitory effect was observed for *Mkl1*, a paralog of *Mkl2* (Supplementary Fig. 4). The repression of Foxo1/3/4 activity in the PI3K/AKT inhibited state by Mkl1/2 suggests that Mkl1 and Mkl2 are repressors of Foxo1/3/4 independent of the PI3K/AKT pathway.

Mkl2 repression of Foxo1 relies on direct interaction, not post-translational modification

We next investigated whether the repression of Foxo1/3/4 by Mkl1/2 is dependent on a protein-protein interaction. Co-immunoprecipitation experiments confirmed the binding of Foxo1/Mkl2 and Foxo1/Mkl1 (Fig. 2a-b). Split luciferase assay experiments also

confirmed the binding of all combinations of Foxo1/3/4 and Mkl1/2 (Fig. 2c-d, Supplementary Fig. 5a-d). We then used the *Foxo1* deletion construct to determine to which regions of the Foxo1 protein Mkl2 binds. Foxo1 lacking the forkhead domain showed significantly reduced binding to Mkl2 (Fig. 2e). The forkhead domain is required for Foxo1 to bind to cis-regulatory elements on genomic DNA in the nucleus. Thus, Mkl2 may repress the transcriptional activity of Foxo1 by inhibiting its ability to bind to DNA. When the nuclear translocation of Mkl1/2 was inhibited using CCG-1423[35], the binding of Mkl1/2 and Foxo1 was significantly reduced, suggesting that Mkl1/2 binds to Foxo1 in the nucleus (Fig. 2f, Supplementary Fig. 5e). Split luciferase experiments using a series of *Mkl2* deletion constructs showed that the transactivation domain (TAD) of Mkl2 alone still bound to Foxo1 (Fig. 2g). Indeed, the TAD domain of Mkl2 alone was able to largely repress the transcriptional activity of Foxo1 (Fig. 2h). Furthermore, the TAD domain showed an inhibitory effect on the fusion protein of the forkhead domain of Foxo1 and VP16 (Fig. 2i), indicating that the TAD domain of Mkl2 binds to the DNA binding domain of Foxo1 and inhibits the transcriptional activity of Foxo1. Thus, repression of FoxO transcriptional activity by Mkl1/2 is not achieved by post-translational modifications but by repressive interactions with the DNA binding domain of FoxO.

Mkl1/2 regulates Foxo1 activity in preadipocytes

The reduction in WAT observed in *Mkl2* KO mice was investigated from the perspective of preadipocyte differentiation defects due to Foxo1 overactivation[12]. Foxo1 has been reported to repress both the initiation of *Pparγ* expression and its transcriptional activity[9-11]. Knockdown of *Mkl2* in 3T3-L1 preadipocytes using siRNA significantly impaired differentiation into mature adipocytes and suppressed the induction of expression of *Pparγ* and white adipose differentiation markers (Fig. 3a-c). Furthermore, the transcriptional activity of Pparγ was repressed by Foxo1, but this repression was rescued by Mkl2 (Supplementary Fig. 6a). Mkl1 also showed a similar effect on the activity of Pparγ and the differentiation of adipocytes (Supplementary Fig. 6b, 7a-d). Adenoviral overexpression of *Foxo1* in 3T3-L1 preadipocytes suppressed adipocyte differentiation. However, co-expression of *Mkl2* or *Mkl1* partially rescued the differentiation defect caused by *Foxo1* overexpression (Fig. 3d). Similar to treatment with LY294002, a PI3K inhibitor, adipocyte differentiation was also significantly suppressed in the presence of CCG-1423[35], which inhibits Mkl1/2 nuclear translocation (Fig. 3e). *Pparγ* expression was also suppressed in the presence of CCG-1423 (Fig. 3f), indicating that Mkl1/2 regulate preadipocyte differentiation by repressing Foxo1 activity in the nucleus.

We next investigated how Mkl1/2 responded to Foxo1 activation by analyzing

their subcellular localization. Adenoviral expression of *Foxo1* and *Mkl2* fused to fluorescent proteins in 3T3-L1 preadipocytes showed that both Foxo1 and Mkl2 were mainly localized in the cytoplasm (Fig. 3g). However, constitutively active mutants of Foxo1 (ADA) altered its localization to the nucleus. Surprisingly, although the Mkl2 protein remained wild-type, its localization also changed to the nucleus. Thus, in response to the localization of Foxo1, the subcellular localization of Mkl2 was determined (Fig. 3g). Similar localization changes responding to Foxo1 activity were also observed for Mkl1 (Supplementary Fig. 7e).

Next, time-lapse imaging was performed to visualize these localization changes upon Foxo1 activation over time. When the PI3K inhibitor wortmannin was added, Foxo1 rapidly translocated to the nucleus, followed by increased nuclear localization of Mkl2 (Fig. 3h, Supplementary Movie 1). Similar changes in Mkl2 and Mkl1 localization were observed with LY294002, another PI3K inhibitor (Supplementary Fig. 8a-b). In addition, both Mkl1 and Mkl2 accumulated in the nucleus when nuclear export was inhibited with leptomycin B (Fig. 3i, Supplementary Fig. 8c). These results suggest that Mkl1 and Mkl2 are constantly shuttling between the cytoplasm and the nucleus, and once Foxo1 is activated, they remain in the nucleus and modulate Foxo1 activity.

Atrogenes and *Mkl1* expression are always inversely correlated in various muscle atrophies

In skeletal muscle, various factors promote the nuclear translocation of Foxo1, Foxo3 and Foxo4 and strongly induce the expression of atrogenes such as *atrogin-1* and *MuRF1*, leading to muscle protein degradation and even muscle atrophy[13-16]. Therefore, we investigated whether *Mkl1/2* are involved in skeletal muscle homeostasis by regulating the activity of Foxo1, Foxo3 and Foxo4. First, we analyzed the subcellular localization of Mkl1/2 in C2C12 myotubes by adenoviral expression of *Mkl1* or *Mkl2* fused to eGFP. Mkl1 was exclusively localized in the nucleus, whereas Mkl2 was localized in the cytoplasm (Fig. 4a). This suggests that Foxo1/3/4 activity in skeletal muscle may be under constant repression by Mkl1. We further investigated changes in *Mkl1/2* during the onset of muscle atrophy. We selected to examine a variety of muscle atrophies with different causes, such as aging, sciatic denervation, fasting, steroid administration and cancer cachexia. During aging, the expression of FoxO target genes such as *atrogin-1* and *MuRF1* was significantly increased, while the expression of *Mkl1* was decreased. The expression of *Mkl2* did not change with aging. The expression of *Foxo1* and *Foxo3* was increased, but the expression of *Foxo4* was unchanged (Fig. 4b).

We also re-analyzed comprehensive RNA-seq data from mouse gastrocnemius

muscle at 8, 18, 22, 24, 26, and 28 months[36]. Mice are thought to develop sarcopenia spontaneously after about 26 months of age. Indeed, the expression of atrogenes, *Foxo1* and *Foxo3* were significantly upregulated in mice after this age, while *Mkl1* expression was significantly downregulated (Supplementary Fig. 9). These data also revealed that there is a strong inverse correlation between the expression of atrogenes and *Mkl1* (Fig. 4c). More surprisingly, between *Mkl1* and *Foxo1* or *Foxo3*, an even stronger inverse correlation was observed (Fig. 4d). Since *Foxo4* expression increased only slightly with age, a weak inverse correlation with *Mkl1* was observed (Fig. 4b, d, Supplementary Fig. 9).

Similarly, an inverse correlation between atrogene and *Mkl1* expression was observed in other models of muscle atrophy. In sciatic nerve denervation-induced muscle atrophy, a significant increase in the expression of atrogenes was observed in the tibialis anterior and gastrocnemius muscles on the side where the sciatic nerve was denervated, 3 and 7 days after treatment. In contrast, *Mkl1* expression was significantly reduced in the same muscles (Fig. 4e, Supplementary Fig. 10a). There were strong inverse correlations between atrogenes and *Mkl1* expression in this model (Fig. 4f, Supplementary Fig. 10b). In addition, increased expression of *Foxo1* and *Foxo3*, but not *Foxo4*, was observed (Fig. 4e).

Similar inverse correlations between *Mkl1* and atrogenes, *Foxo1* or *Foxo3* expression were also observed in muscle atrophy induced by fasting, dexamethasone administration and cancer cachexia. When mice were fasted for 24 hours, increased expression of atrogenes, *Foxo1* and *Foxo3* was observed in the gastrocnemius muscle, while *Mkl1* expression was significantly decreased (Supplementary Fig. 11). Similar changes in gene expression were also observed in mouse muscle as early as 16 hours after intraperitoneal administration of dexamethasone (Supplementary Fig. 12). We also examined gene expression changes in skeletal muscle associated with cancer cachexia and found a similar inverse correlation between *Mkl1* and atrogenes, *Foxo1* and *Foxo3* (Supplementary Fig. 13). This analysis was performed by re-analyzing the data stored in the Gene Expression Omnibus (GEO) database[37]. Thus, in all the muscle atrophy models that we could examine, the expression of *Mkl1* was always repressed after the onset of muscle atrophy.

To determine whether the decreased expression of *Mkl1* was a consequence of activation of the muscle atrophy signaling pathway, we examined endogenous *Mkl1* expression during muscle catabolism (Supplementary Fig. 14). In C2C12 myotubes, addition of hydrocortisone, dexamethasone or adenoviral overexpression of *Foxo1* and *Foxo3* did not reduce endogenous *Mkl1* expression. PI3K inhibition also failed to reduce

Mkl1 expression. These data suggest that suppression of endogenous *Mkl1* expression may occur independently of activation of the GR/FoxO pathway or inhibition of the PI3K/AKT pathway.

Mkl1 and _Mkl2_ repress the induction of atrogene expression in the skeletal muscle

We then investigated whether *Mkl1* and *Mkl2* could inhibit FoxO-induced muscle atrophy in cultured myotubes. Since little upregulation of *Foxo4* was observed in the muscle atrophy models we examined, we used adenoviral expression of *Foxo1* or *Foxo3* in myotubes to induce muscle atrophy. Overexpression of *Foxo1* or *Foxo3* in myotubes increased the expression of atrogenes such as *atrogin-1* and *MuRF1*. This induction was suppressed by *Mkl1* or *Mkl2*, even in the presence of the PI3K inhibitor, LY294002 (Fig. 5a-d). Notably, *Mkl1* had a stronger inhibitory effect on atrogene expression than *Mkl2*, which may reflect differences in subcellular localization of Mkl1 and Mkl2 in skeletal muscle cells (Fig. 4a). As mentioned above, we have shown that Mkl2 binds to the forkhead domain of Foxo1 (Fig. 2e). Therefore, we performed chromatin immunoprecipitation of Foxo3 in myotubes to determine whether FoxO binding to the cis-regulatory region of downstream atrogenes is altered in the presence of Mkl1 or Mkl2. From the ChIP-Atlas database[38], regions with high scores in previous Foxo3 ChIP-seq data were selected as Foxo3 binding sites. Foxo3 binding was observed at these sites near the *atrogin-1* and *MuRF1* genes, but co-expression of *Mkl1* or *Mkl2* reduced Foxo3 binding at these sites (Supplementary Fig. 15). This suggests that Mkl1 and Mkl2 bind to Foxo3 to inhibit its DNA binding in skeletal muscle.

Similarly, the expression of atrogenes induced by glucocorticoids was also suppressed by *Mkl1* or *Mkl2* (Fig. 5e). Surprisingly, *Mkl1* also blocked the induction of *Foxo3* expression induced by GR activation (Fig. 5f). We found that Mkl1 and Mkl2 directly bind to GR and repress its transcriptional activity (Supplementary Fig. 16). Thus, Mkl1 and Mkl2 repress both FoxO activity and GR activity in the GR/FoxO axis.

In contrast to overexpression of *Mkl1* or *Mkl2*, knockdown of *Mkl1* or *Mkl2* resulted in increased expression of *atrogin-1* and *MuRF1* (Fig. 5g-h, Supplementary Fig. 17). Although *MuRF1* mRNA changes by *Mkl1* or *Mkl2* knockdown were relatively small, significant upregulation was observed at the protein level. Similarly, inhibition of nuclear localization of Mkl1 and MKl2 by CCG-1423 alone resulted in increased expression of *atrogin-1* and *MuRF1*, and dual inhibition of Mkl1/2 nuclear localization and PI3K/AKT pathway with CCG-1423 and LY294002 synergistically and strongly increased expression of atrogenes (Fig. 5i-j). This result indicates that the suppression of Foxo1/3/4 by Mkl1/2 is independent of the PI3K/AKT pathway.

Mkl1/2 supplementation inhibits skeletal muscle atrophy

To test the protective effects of *Mkl1* and *Mkl2* against muscle atrophy, we examined the size of C2C12 myotubes. Overexpression of *Foxo1* or *Foxo3* caused severe atrophy of the myotubes. However, when *Mkl1* or *Mkl2* was co-expressed with *Foxo1* or *Foxo3*, no such atrophy was observed (Fig. 6a). Based on the two facts that *Mkl1* and *Mkl2* have repressive effects on FoxO transcriptional activity and that *Mkl1* is drastically reduced at the onset of muscle atrophy, we hypothesized that if *Mkl1* expression could be compensated during muscle atrophy, it might be possible to confer resistance to skeletal muscle atrophy. A modified adeno-associated virus (MyoAAV.2A) with strong muscle tropism has been reported[39]. Using this MyoAAV.2A, we attempted to express *Mkl1* in muscles throughout the body. First, MyoAAV.2A encoding *AkaLuc-eGFP* was administered systemically to mice and expression was confirmed. AkaLuc-eGFP was successfully induced in muscles such as gastrocnemius and tibialis anterior, as well as in the heart (Supplementary Fig. 18). Expression reached a plateau approximately 2 weeks after administration. We then administered MyoAAV.2A encoding *Mkl1* to mice. Significant cardiac hypertrophy was observed following administration of AAV encoding *Mkl1* at doses greater than 2×10^{11} vg (Supplementary Fig. 19). Therefore, we had to administer lower doses of AAV to the mice to assess skeletal muscle changes. After 10 weeks of AAV treatment, the muscles of mice treated with MyoAAV.2A encoding *Mkl1* were heavier than those of the untreated group (Fig. 6b).

We then treated the mice with dexamethasone and examined changes in the expression of atrogenes and Foxo1/3/4. Dexamethasone-induced upregulation of *atrogin-1* could not be suppressed by treatment with MyoAAV.2A encoding *Mkl1*, but *MuRF1* and other atrogenes were suppressed (Fig. 6c). In addition, dexamethasone-induced upregulation of *Foxo1* and *Foxo3* could be blocked by *Mkl1* (Fig. 6c). We then examined whether the fasting-induced expression of atrogenes was altered by *Mkl1* supplementation. In the *Mkl1*-supplemented gastrocnemius muscle, the fasting-induced increase in *Foxo1* and *Foxo3* expression was significantly suppressed (Fig. 6d). Although the induction of *atrogin-1* and *MuRF1* expression was barely suppressed, the increased expression of several other atorogenes was significantly suppressed (Supplementary Fig. 20). Thus, *Mkl1* supplementation in skeletal muscle showed a protective effect against the induction of skeletal muscle atrophy.

Exercise activates *Mkl1/2* by promoting nuclear accumulation of Mkl2 and increasing *Mkl1/2* expression in skeletal muscle

As mentioned above, *Mkl1* expression is invariably reduced at the onset of muscle atrophy (Fig. 4b, e, Supplementary Fig. 9-13), reducing its inhibitory effect on GR and Foxo1/3/4. Finally, as an opposite situation, we investigated whether *Mkl1/2* is activated during the anabolic process or during the inhibition of catabolism in skeletal muscle. Exercise is known to induce muscle hypertrophy and is also known to inhibit muscle atrophy. Therefore, we investigated whether skeletal muscle contraction and exercise affect *Mkl1/2*.

Mkl2 localizes to the cytoplasm in myotubes (Fig. 4a). Interestingly, a nuclear translocation of Mkl2 was observed in response to contraction in myotubes (Fig. 6e, Supplementary Movie 2). This suggests that myotube contraction increases the inhibitory effect of *Mkl2* on muscle atrophy in skeletal muscle cells. Similarly, when the gastrocnemius muscle was excised immediately after treadmill exercise and cellular proteins were fractionated, the amount of nuclear Mkl2 protein was significantly increased (Fig. 6f). In addition, we found that four weeks of treadmill exercise in mice increased skeletal muscle expression of *Mkl1* and *Mkl2* (Fig. 6g), as in human skeletal muscle after long-term resistance training[40]. These results suggest that exercise activates *Mkl1/2* in skeletal muscle, both by increasing nuclear accumulation of Mkl2 and by increasing expression levels of *Mkl1* and *Mkl2*. Thus, some of the beneficial effects of exercise may involve *Mkl1* and *Mkl2*.

DISCUSSION

In this study, we discovered a novel mechanism of Foxo1/3/4 repression that is independent of the PI3K/AKT pathway. Both Mkl1 and Mkl2 are central to this repression mechanism. Mkl1/2 appear to repress the transcriptional activity of Foxo1/3/4 by inhibiting its ability to bind to DNA. The activity of Foxo1/3/4 was thought to be primarily regulated by post-translational modifications, but the mode of repression by Mkl1/2 is based on direct protein-protein interactions. Regulation of Foxo1/3/4 activity by Mkl1/2 is important for the maintenance of at least two tissues, white adipose tissue and skeletal muscle. The plasticity of these two tissues is strongly affected by aging. It is therefore possible that Mkl1/2 activity decreases with age. Indeed, we observed a significant decrease in *Mkl1* expression in the skeletal muscle of mice as they aged.

In preadipocytes, we have shown that there is a novel mechanism by which Mkl1/2 rapidly responds to Foxo1 activation by shuttling between the cytoplasm and the nucleus. When Foxo1 is activated and accumulates in the nucleus, Mkl1/2 also remains in the nucleus, preventing Foxo1 overactivation and thereby ensuring *Pparγ* expression. In contrast, in skeletal muscle, myocyte contraction promotes nuclear translocation of

Mkl2 and continuous exercise increases *Mkl1/2* expression, indicating that exercise activates *Mkl1/2*. Mkl1/2 inhibits GR/FoxO pathway involved in skeletal muscle atrophy (Supplementary Fig. 21). Surprisingly, in all muscle atrophy models studied, there was a mechanism by which *Mkl1* expression was repressed with the onset of muscle atrophy. This suggests that the downregulation of *Mkl1* is essential for the progression of muscle atrophy and that *Mkl1* is a potent inhibitor of muscle atrophy. Indeed, *Mkl1* showed a stronger inhibitory effect on atrogenes, Foxo1/3/4 and GR.

It is clear that *Mkl2* is required for WAT plasticity, since a decrease in WAT is observed in *Mkl2* KO mice. However, our results are in conflict with several reports on the effects of *Mkl1* on adipogenesis. Nobusue et al. reported that *Mkl1* negatively regulates white adipocyte differentiation by repressing the transcriptional activity of *Pparγ*[41]. McDonald et al. reported that loss of *Mkl1* in mesenchymal stem cells promotes lineage commitment to brown adipocytes[42]. *Mkl1* KO mice appeared to have reduced amounts of subcutaneous and visceral WAT. At the same time, the expression of thermogenic genes such as *Ucp1* was increased in subcutaneous WAT[42]. In contrast, our results show that Mkl1, like Mkl2, can also repress the transcriptional activity of Foxo1, and that knockdown of *Mkl1* in preadipocytes significantly impairs *Pparγ* expression and white adipocyte differentiation. Adipogenesis consists of several steps including multipotent mesenchymal precursors, preadipocyte commitment, growth arrest, clonal expansion, terminal differentiation and maturation. During this process, Foxo1 switches between activated and inactivated states, and the onset of *Pparγ* expression corresponds to the second inactivation of Foxo1[43]. The role of *Mkl1* may change at each step, but at least with respect to the repression of *Pparγ* by *Foxo1*, *Mkl1* may be as necessary as *Mkl2* for white adipocyte differentiation. Incidentally, it has been reported that Foxo1 activation increases *Ucp1* expression in WAT[44]. Thus, the increased expression of *Ucp1* in *Mkl1* KO mice may be partly due to the activation of Foxo1.

Srf is already known to be important for skeletal muscle development[45]. The present study showed that its cofactor *Mkl1* and *Mkl2* play a protective role against muscle protein degradation by suppressing Foxo1/3/4 and GR independently of *Srf*. It is very interesting that *Srf* and its cofactors are responsible for both skeletal muscle development and inhibition of atrophy. In addition, *Mkl1* and *Mkl2* are activated by exercise. It is known that exercise is effective in preventing sarcopenia and it is now clear that *Mkl1* and *Mkl2* are involved in this molecular mechanism. In the future, if we can develop agents that can increase the expression of *Mkl1* or *Mkl2*, or promote the nuclear localization of Mkl2 in skeletal muscle, it is expected that such agents will mimic exercise and inhibit muscle atrophy.

We used an adeno-associated virus (MyoAAV.2A) to express *Mkl1* in the skeletal muscle of mice. There was an upper limit to the amount of virus that could be administered because higher levels of *Mkl1* expression in the myocardium caused cardiac hypertrophy. Despite the small amount of virus compared to other studies, *Mkl1* was able to suppress the induction of the expression of many atrogenes, *Foxo1* and *Foxo3* in skeletal muscle, resulting in muscle hypertrophy. A more potent inhibitory effect on muscle atrophy may be achieved by using an adeno-associated virus with a more skeletal muscle-specific promoter. Incidentally, overactivation of FoxO proteins has been reported in dilated cardiomyopathy (DCM) caused by *Lmna* mutations[34]. The nuclear localization of Mkl1 is markedly attenuated in *Lmna* deficiency or N195K mutant[33], suggesting that *Mkl1/2* dysfunction may be involved in the cause of these DCM. *Foxo1* overactivation in the myocardium has also been implicated in the pathogenesis of diseases other than DCM. For example, doxorubicin, an anticancer drug, has been reported to increase the transcriptional activity of Foxo1 in the myocardium, leading to myocardial atrophy[46]. Therefore, inhibition of Foxo1 by Mkl1 or Mkl2 may be a potential therapeutic candidate for anthracycline-induced cardiac injury.

Author Contributions

A.K. designed and performed the experiments and analyzed the data. A.K., K.H., R.S. and T.O. discussed and interpreted the analyses. The manuscript was written by A.K and edited by all authors.

Acknowledgments

We thank T.O., K.H., and R.S. laboratory members for technical assistance, comments on the manuscript, and scientific discussions. We thank Masafumi Inui for scientific discussions. We thank the Institute of Development, Aging and Cancer and the Kobe Biomedical Research Foundation for providing the aged mice. This work was supported by JSPS Grant-in-Aid for Scientific Research 21K11386 (A.K.); The Ito Foundation (A.K.); Daiwa Securities Foundation (A.K.); CASIO Science Promotion Foundation (A.K.); TOBE MAKI Scholarship Foundation (A.K.); and AMED 19gm0810001 (T.O.).

MATERIALS AND METHODS

Mouse experiments

ES cells (MrtfbTM1a(KOMP)Mbp) were purchased from KOMP and used to generate chimeric mice. MrtfbTM1a(KOMP)Mbp mice were sequentially crossed with CAG-FRT and CAG-Cre mice to generate heterozygous mice lacking exons 11 and 12 of the *Mkl2* gene. The heterozygous mice were maintained in the C57BL/6N and ICR mouse strains, and *Mkl2* knockout mice lacking both alleles were generated by heterosis between the two strains. C57BL/6J mice (including aged mice) used in other animal experiments were obtained from CLEA Japan, Inc. Some other aged mice were also provided by the Institute of Development, Aging and Cancer and the Kobe Biomedical Research Foundation through the National BioResource Project of the Ministry of Education, Culture, Sports, Science and Technology.

Long-term exercise training of mice was performed as follows: 10-week-old C57BL/6J male mice were exercised on a treadmill for 60 minutes per day for 4 weeks. Forced running was started at a speed of 15 m/min, and the speed was increased by 1 m/min every 10 min until the speed reached 20 m/min. After 4 weeks of training, the mice were dissected and analyzed for gene expression in the gastrocnemius muscle. For subcellular fractionation of muscle protein, gastrocnemius muscle from mice trained on a treadmill for 3 h was fractionated into cytoplasm and nucleus using the Subcellular Protein Fractionation Kit for Tissues (Thermo Fisher Scientific).

In the denervation-induced muscle atrophy model, the sciatic nerve was denervated in the right hindlimb of 10-week-old C57BL/6J male mice, and the right and left gastrocnemius and tibialis anterior muscles were harvested 3 and 7 days after denervation. For fasting-induced muscle atrophy, 9-week-old C57BL/6J male mice were fasted for 24 hours. After fasting, mice were euthanized and gastrocnemius muscles were harvested.

Dexamethasone sodium phosphate was dissolved in PBS and administered intraperitoneally to mice. AAV was also dissolved in PBS and administered to mice via the tail vein. Transgene expression after AAV administration was confirmed by measuring bioluminescence using the IVIS Imaging System LuminaII or by eGFP fluorescence.

The mouse experiments were approved by Institutional Laboratory Animal Care and Use Committee of Tohoku University and Safety Committee for Recombinant DNA Experiments of Tohoku University.

Reagents and antibodies

The reagents used in this study were as follows: Dexamethasone, IBMX, and insulin solution were from Sigma-Aldrich; hydrocortisone was from PromoCell; CCG-1423 and leptomycin B were from Cayman Chemical; MG-132, LY-294002, doxycycline hydrochloride n-hydrate, and dexamethasone sodium phosphate were from Fujifilm Wako Chemicals.

The following antibodies were used in this study Anti-PPARγ (C26H12, #2435), anti-HSL (#4107), anti-perilipin-1 (D418, #3470), anti-lamin A/C (#2032), anti-HA tag (C29F4, #3724), and normal rabbit IgG (#2729) from Cell Signaling Technology; anti-atrogin-1 (F-9, sc-166806) and anti-MuRF1 (C-11, sc-398608) from Santa Cruz Biotechnology; anti-GAPDH (M171-7), anti-β-actin (PM053-7), anti-DDDDK-tag (PM020-7) and anti-HA-tag (561-7) from MBL; anti-beta-tubulin (HRP-66240) from Proteintech.

The siRNA used in this study (27mer DsiRNA) were pre-designed products from Integrated DNA Technologies: *Mkl1* siRNA #1 (#106160699), *Mkl1* siRNA #2 (#106037572), *Mkl1* siRNA #3 (#106037569), *Mkl2* siRNA #1 (#105942460), *Mkl2* siRNA #2 (#105942457), *Mkl2* siRNA #3 (#105942454), and Negative Control DsiRNA (#51-01-14-04).

Plasmids and cosmids

The *Foxo1/3/4* responsive luciferase reporter plasmid was constructed by inserting six FoxO REs (FoxO responsive elements) into pGL4.23 (Promega). The following sequence, 5′-TGTTTGGCCGCTCTGTTTACGGCAGCAAGAGGATCTGTTTTTGGCCGCTTGTTTACGGCAAGTAAACA-3′, was used as the FoxO RE sequence. Similarly, a *Pparγ* responsive luciferase reporter was created by incorporating three PPRE (*Pparγ* responsive elements) into pGL4.23. The single PPRE sequence is 5′-AGGGGACCAGGACAAAGGTCACGTTCGGGA-3′. A glucocorticoid receptor responsive luciferase reporter was created by incorporating four glucocorticoid receptor responsive elements (GREs) into pGL4.23. The single GRE sequence is 5′-GGTACATTTTGTTCT-3′. The second of the four GREs was placed in the antisense orientation.

Protein coding sequences (CDS) for *Foxo1*, *Foxo3*, *Foxo4*, and glucocorticoid receptor (*Nr3c1*) were amplified by PCR from mouse cDNA. The CDSs for *Mkl1* and *Mkl2* were synthesized as DNA fragments, and these codons were optimized (Integrated DNA Technologies). These CDSs were cloned into mammalian expression vectors (pcDNA3.1) or NanoBiT PPI starter system vectors (pBiT1.1-N, pBiT1.1-C, pBiT2.1-N and pBiT2.1-C).

Tet-On adenoviral cosmid vector was produced by the following procedure: The multicloning site of pTetOne vector (TaKaRa) was modified to retain a SwaI recognition sequence. The entire transgene expression regulatory region of the pTetOne vector was inserted into the pAxcwit2 cosmid vector to create the pAxcwit2-TetOne vector. Finally, transgenes such as *Foxo1/3/4* or *Mkl1/2* were inserted into pAxcwit2-TetOne using the SwaI site.

AAV transfer plasmids were constructed by removing all sequences between the ITRs of the pAAV-CMV vector (TaKaRa) and instead inserting the Mhck7 promoter, transgene, and SV40 polyA sequence. DNA templates for Mhck7 promoter, *AkaLuc* and *Mkl1* were prepared by gene synthesis (Integrated DNA Technologies). The Rep/Cap plasmid encoding the MyoAAV.2A capsid was generated by modification of pUCmini-iCAP-PHP.S by inverse PCR[47]. The hypervariable region VIII sequence SAQQAVRTSL was replaced with GPGRGDQTTL. pUCmini-iCAP-PHP.S was a gift from Viviana Gradinaru (Addgene plasmid # 103006 ; http://n2t.net/addgene:103006 ; RRID:Addgene_103006). The helper plasmid was pHelper (TaKaRa).

Cell culture

3T3-L1 cells (ATCC) were maintained in DMEM (Nacalai Tesque) containing 10% calf serum (Gibco). For differentiation into adipocytes, 3T3-L1 cells were cultured to confluence, then the medium was changed and the cells were cultured for an additional 48 hours. To initiate differentiation, the medium was replaced with differentiation medium (90% DMEM, 10% FBS, 1mM sodium pyruvate, 1μM dexamethasone, 0.5mM IBMX and 1μg/mL insulin). After 48 hours, the differentiation medium was replaced with maintenance medium (90% DMEM, 10% FBS, 1 mM sodium pyruvate and 1μg/mL insulin), which was then changed every 48 hours.

C2C12 cells (ATCC) were seeded in dishes coated with Geltrex™ LDEV-Free Reduced Growth Factor Basement Membrane Matrix (Thermo Fisher Scientific) and maintained in DMEM (Nacalai Tesque) containing 10% FBS (Gibco). For differentiation into myotubes, the culture medium was replaced with DMEM containing 2% horse serum (Gibco) after C2C12 cells reached confluence. Three days after the induction of differentiation, adenovirus was added to the medium to infect the myotubes with adenovirus, and the next day, doxycycline (Wako) was added to induce transgene expression. 293FT cells were purchased from Thermo Fisher Scientific and maintained in DMEM (Nacalai Tesque) containing 10% FBS (Gibco).

Electrical pulse stimulation

Electrical pulse stimulation was applied to well-differentiated myotubes on day 5 of differentiation. Two graphite plates were inserted into the wells and a constant voltage bipolar square pulse was generated between the graphite plates at 1 Hz using a C-Pace EM (IonOptix) to contract the myotubes.

Luciferase assays

Luciferase reporter and plasmids encoding each gene were transfected into 293FT cells (Thermo Fisher Scientific) using Polyethylenimine Max (MW 40,000) (Polysciences). If necessary, LY294002 or dexamethasone was added 24 hours after transfection. Forty-eight hours after transfection, cells were harvested and lysed. D-luciferin and ATP were added to the cell extract and the luminescence intensity was measured using a GloMax® Discover Microplate Reader (Promega).

Detection of protein-protein interactions

For co-immunoprecipitation assays, 293FT cells were transfected with plasmids encoding FLAG-tagged and/or HA-tagged proteins using Polyethylenimine Max (MW 40,000) (Polysciences). After 48 hours, cells were harvested and sonicated in lysis buffer (50 mM HEPES (pH 8.0), 0.3 M NaCl, 0.2% NP40, protease inhibitor). After centrifugation, ANTI-FLAG M2 Affinity Gel (Sigma A2220) was added to the supernatant and incubated at 4°C for 4 hours. After washing the beads, SDS sample buffer was added and the immunoprecipitated proteins were analyzed by Western blotting.

Protein-protein interactions between Mkl1/2 and Foxo1/3/4 or glucocorticoid receptor were also measured using NanoBiT® PPI Starter Systems (Promega). 293FT cells (Thermo Fisher Scientific) were seeded in 96-well white wall microplates and co-transfected with LgBiT and SmBiT plasmids. The SmBiT-HaloTag plasmid was used for background measurements. At 24 hours post-transfection, luminescent substrate was added and luminescence was measured using the GloMax® Discover Microplate Reader (Promega).

Gene expression analysis

RNA extraction was performed as follows. For RNA extraction from mice, mice were euthanized and white adipose tissue or skeletal muscle was isolated. TRIzol reagent (Thermo Fisher Scientific) was added. Tissues were homogenized using Micro Smash MS-100R (TOMY). For RNA extraction from cultured cells, the FavorPrep Blood/Cultured Total RNA Mini Kit (FAVORGEN) was used. In both cases, RNA extraction was performed according to the manufacturer's instructions. Purified RNA was

analyzed by microarray (3D-Gene, TORAY) or RT-qPCR. For RT-qPCR, purified RNA was reverse transcribed using ReverTra Ace® (TOYOBO). Gene expression was measured using SsoAdvanced Universal SYBR Green Supermix (BIO-RAD) with primer sets specific for each cDNA. Most primers used for RT-qPCR were pre-designed from PrimerBank, but primers for 18S rRNA, Mkl2 and ChIP-qPCR were designed using Primer-BLAST (NIH). The primers used are listed in Supplementary Table 2. Oligonucleotides were synthesized by Integrated DNA Technologies. The gene expression profiles of gastrocnemius muscle in aging or cancer cachexia were re-analyzed from RNA-seq data (GEO accession numbers: GSE145480 or GSE65936) in the GEO database. For upstream analysis, Ingenuity® Pathway Analysis was used to analyze the list of genes with variable expression obtained from the microarray.

Viral vector production

For adenovirus production, the adenovirus genome was excised from the cosmid vector using restriction enzymes BspT104I or PacI, then excised DNA was purified and transfected into Adeno-X 293 cells (TaKaRa). When late CPE was observed, cells and culture medium were collected and virus was extracted by freezing and thawing six times. In addition, the cycle of cell infection and virus extraction was repeated twice to produce high-titer adenovirus solution.

Adeno-associated virus (MyoAAV.2A) was produced using the AAV-MAX Helper-Free AAV Production System Kit (Thermo Fisher Scientific). At 72 hours post-transfection, AAV was extracted with citrate buffer (55 mM citric acid, 55 mM sodium citrate, 800 mM NaCl). The extract was neutralized with HEPES (pH 8.0) and precipitated with PEG 8000. The pellet containing AAV was resuspended and treated with Benzonase® (MERCK) for nucleic acid digestion. For further purification, density gradient ultracentrifugation was performed using OptiPrep. Purified AAV was replaced with buffer in PBS and viral genome (vg) content was determined by RT-qPCR.

artificial microRNA

Artificial microRNAs (miRNAs) to repress the expression of *Mkl1* or *Mkl2* were incorporated into cosmid vectors for adenovirus. A miRNA cluster consisting of t hree miRNAs is located in the 3' UTR of eGFP, whose expression is regulated by the Tet-ON promoter. The sequence of each miRNA is shown below. *Mkl1* m iRNA #1: 5'-CTGTTCAAAGGCGGCATGATCCCTGTTTTGGCCACTGACTGACA GGGATCACCGCCTTTGAACAG-3', *Mkl1* miRNA #2: 5'-CTGATTTCTCGCTGG CAGACTTGGGTTTTGGCCACTGACTGACCCAAGTCTCAGCGAGAAATCAG-3',

Mkl2 miRNA #1: 5'-CTGAGAACTGCGAGACAACGTTCTGTTTTGGCCACTGACTGACAGAACGTTCTCGCAGTTCTCAG-3', *Mkl2* miRNA #2: 5'-CTGAGACCTTTCTGACTGGCTGAGGTTTTGGCCACTGACTGACCTCAGCCACAGAAAGGTCTCAG-3'.

Statistics

Measurements for each experiment are presented as mean ± SD. Statistical significance was determined by Student's t-test, Dunnett's test, or Tukey's test using JMP statistical software, with a p-value < 0.05 considered significant.

FIGURE LEGENDS

Fig. 1

a, Body weight of *Mkl2* KO mice and littermates. Data are presented as box plots (males: WT: n=6, Ht: n=17, KO: n=7, females: WT: n=23, Ht: n=33, KO: n=16). **b-c**, White adipose tissue (WAT) of *Mkl2* KO mice and their littermates. Whole abdomen (**b**) and inguinal WAT (**c**). **d**, Gastrocnemius muscle of *Mkl2* KO mouse and littermate. **e-f**, Tissue weight of *Mkl2* KO mice and their littermates. Inguinal WAT (**e**) and gastrocnemius muscle (**f**). Data are presented as box plots (WT: n=11, Ht: n=11, KO: n=6). **g**, Prediction of upstream regulatory transcription factors based on differentially expressed genes in inguinal WAT of *Mkl2* KO mice. **h-i**, Inhibitory effects of Mkl2 on the transcriptional activity of Foxo1, Foxo3 and Foxo4 using luciferase reporters with FoxO response elements in the normal state (**h**) or in the state of PI3K/AKT pathway suppressed by LY294002 treatment (**i**). Data are mean ± s.d. of n = 3 cultures per condition. **a**, **e**, **f**, **h**, **i**, Significance (*$p < 0.05$, **$p < 0.01$, ***$p < 0.001$, or ****$p < 0.0001$) was calculated using Student's t-test (**h**) or Dunnett's test (**a**, **e**, **f**, **i**) for multiple comparisons.

Fig. 2

a-b, Co-immunoprecipitation assay of Foxo1 and Mkl2 (**a**) or Mkl1 (**b**). FLAG-tagged and HA-tagged proteins were expressed in 293FT cells. FLAG-tagged protein was immunoprecipitated using FLAG antibodies. Co-immunoprecipitation was confirmed by detection with HA antibody. **c-d**, Protein-protein interaction (PPI) of Foxo1, Foxo3 and Foxo4 with Mkl2 (**c**) or Mkl1 (**d**) was analyzed using split luciferase (NanoBiT). The relative PPI signal was calculated based on the signal between the LgBiT tagged protein and the SmBiT-Halotag (Lg: LgBiT tag, Sm: SmBiT tag, HT: Halotag). **e**, PPI of Mkl2 with truncated Foxo1 proteins using split luciferase (NanoBiT). **f**, Changes in the interaction of Foxo1 with Mkl1 or Mkl2 by addition of CCG-1423, an inhibitor of nuclear translocation of Mkl2 and Mkl1. **g**, PPI of Foxo1 with truncated Mkl2 proteins. **h-i**, Luciferase assay using a reporter with FoxO responsive elements. Transcriptional activity of Foxo1 (**h**) or forkhead domain of Foxo1 and VP16 fusion protein (**i**) with or without nuclear localized TAD domain of Mkl2. **c-i**, Data are mean ± s.d. of n = 3 cultures per condition. Significance (*$p < 0.05$, **$p < 0.01$, ***$p < 0.001$, or ****$p < 0.0001$) was calculated using Student's t-test (**f**) or Dunnett's test (**c**, **d**, **e**, **g**, **h**, **i**) for multiple comparisons. n.s: not significant.

Fig. 3

a, Oil red O staining of *Mkl2* knockdown 3T3-L1 cells at day 8 of differentiation. After staining, the dye was extracted with isopropanol and quantified by absorbance at 490 nm (right). **b-c**, Expression levels of *Pparγ*, *Plin1* and *Hsl* mRNA (**b**) and protein (**c**) at day 4, 7 and 10 after induction of differentiation of 3T3-L1 cells with or without *Mkl2* knockdown. The mRNA expression is shown as a relative change from the average expression of the control on day 4. **d**, Oil red O staining of 3T3-L1 cells on day 8 of differentiation overexpressing *Foxo1*, *eGFP*, *Mkl1* or *Mkl2*. After staining, the dye was extracted with isopropanol and quantified by absorbance at 490 nm (bottom). **e**, Oil red O staining of 3T3-L1 cells on day 8 of differentiation treated with LY294002 or CCG-1423. After staining, the dye was extracted with isopropanol and quantified by absorbance at 490 nm (right). **f**, *Pparγ* mRNA expression in CCG-1423 treated 3T3-L1 cells on day 4 of differentiation. **g**, Subcellular localization of Mkl2 with Foxo1 or Foxo1(ADA) expression. The percentages of cells showing nuclear and cytoplasmic localization for Foxo1 and Mkl2, respectively, are shown below. (C: cytoplasmic localization, N: nuclear localization). **h**, Localization changes of Foxo1 and Mkl2 after addition of wortmannin, a PI3K inhibitor. Changes in nuclear signal over time are shown below for two cells with representative behavior. **i**, Changes in Mkl2 localization by treatment with or without leptomycin B. **a, b, d-f**, Data are mean ± s.d. of n = 3 cultures per condition. Significance (*$p < 0.05$, ***$p < 0.001$, or ****$p < 0.0001$) was calculated using Student's t-test (**f**) or Dunnett's test (**a**, **d**, **e**) for multiple comparisons.

Fig. 4

a, Mkl1-eGFP and Mkl2-eGFP were expressed in myotubes derived from C2C12 cells and the subcellular localization of each protein was analyzed. To stabilize the protein levels, the myotubes were treated with MG-132. **b**, Altered expression of atrogenes, *Mkl1*, *Mkl2*, *Foxo1*, *Foxo3* and *Foxo4* in the gastrocnemius muscle of young (8 weeks old, n=4) and old (119 weeks old, n=3) C57BL/6J mice. **c-d**, Inverse correlation between the expression levels of *Mkl1* and atrogenes (**c**) or *Foxo1/3/4* (**d**) in the gastrocnemius muscle of mice of different ages. Each point represents DESeq normalized gene expression in the gastrocnemius muscle of one mouse. These data are from a re-analysis of the GEO dataset (GEO accession number: GSE145480). **e**, Altered expression of atrogenes, *Mkl1*, *Mkl2*, *Foxo1*, *Foxo3* and *Foxo4* in the left or right tibialis anterior muscle of mice with sciatic nerve denervation of the right hindlimb. Day is the number of days after sciatic nerve denervation. (n=5) **f**, Inverse correlation of *Mkl1* and atrogene expression levels in the tibialis anterior muscle of mice with right hindlimb sciatic nerve denervation. Each point represents relative gene expression in either the left or right mouse tibialis anterior muscle.

Relative gene expression was calculated based on the average expression in the left leg before sciatic nerve denervation (day 0). **b, e,** Data are mean ± s.d. Significance (*p < 0.05, **p < 0.01, ***p < 0.001, or ****p < 0.0001) was calculated using Student's t-test. n.s: not significant.

Fig. 5

a, b, Inhibitory effect of *Mkl1* or *Mkl2* on mRNA expression of atrogenes induced by *Foxo1* (**a**) or *Foxo3* (**b**) in C2C12-derived myotubes. Adenovirus was used to express *Foxo1*, *Foxo3*, *Mkl1* or *Mkl2*. Ad: Adenovirus vector. **c, d**, Inhibitory effect of *Mkl1* or *Mkl2* on protein expression of atrogenes induced by *Foxo1* (**c**) or *Foxo3* (**d**) in C2C12-derived myotubes. Adenovirus was used to express *Foxo1*, *Foxo3*, *Mkl1* or *Mkl2*. Ad: Adenovirus vector. **e, f**, Inhibitory effect of *Mkl1* or *Mkl2* on atrogenes (**e**) and *Foxo3* (**f**) mRNA expression induced by glucocorticoid analogues in C2C12-derived myotubes. Adenovirus was used to express *Mkl1* or *Mkl2*. Ad: Adenovirus vector. **g, h,** Changes in mRNA (**g**) or protein (**h**) expression of atrogenes when *Mkl1* or *Mkl2* is suppressed in C2C12-derived myotubes. Knockdown was achieved by infection with adenoviruses expressing artificial microRNAs (miRNAs) against *Mkl1* or *Mkl2*. **i, j,** Altered mRNA (**i**) or protein (**j**) expression of atrogenes in C2C12-derived myotubes in the presence of the PI3K inhibitor LY294002 and/or the Mkl1/2 nuclear translocation inhibitor CCG-1423.
a, b, e, f, g, i, Data are mean ± s.d. of n = 3 cultures per condition. Significance (**p < 0.01, ***p < 0.001, or ****p < 0.0001) was calculated using Dunnett's test (**a**, **b**, **g**) or Tukey's test (**e**, **f**, **i**) for multiple comparisons. n.s: not significant.

Fig. 6

a, Suppression of muscle atrophy by expression of *Mkl1* or *Mkl2* in C2C12-derived myotubes in which muscle atrophy was induced by expression of *Foxo1* or *Foxo3*. Adenovirus was used to express *Foxo1*, *Foxo3*, *Mkl1* or *Mkl2* in the myotube. Ad: Adenovirus vector. **b**, Gastrocnemius muscle of mice 12 weeks after administration of 1×10^{11} vg of MyoAAV.2A (Mhck7-*Mkl1*) via tail vein. (Control: n=3, AAV: n=4) **c**, Comparison of gene expression of atrogenes, *Foxo1*, *Foxo3* and *Foxo4* in gastrocnemius muscle 16 hours after administration of dexamethasone sodium phosphate (Dex). Dex was administered intraperitoneally to mice 12 weeks after MyoAAV.2A (Mhck7-*Mkl1*) administration via the tail vein. Data are mean ± s.d. (n= 7-8). **d**, Comparison of *Foxo1*, *Foxo3* and *Foxo4* expression in gastrocnemius muscle of mice expressing *Mkl1* in muscle by MyoAAV.2A and fasted for 24 hours. Data are mean ± s.d. (n= 7-8). **e**, Changes in the subcellular localization of Mkl2 due to contraction of myotubes induced by electrical

pulse stimulation (EPS). **f**, Subcellular localization of Mkl2 in the gastrocnemius muscle before and after treadmill exercise in C57BL/6J mice. **g**, Changes in *Mkl1* and *Mkl2* expression in gastrocnemius muscle after 4 weeks of treadmill exercise in C57BL/6J mice (Sed: sedentary, n=3, Exc: exercise, n=3). **b-d**, **g**, Significance (*$p < 0.05$, **$p < 0.01$, ***$p < 0.001$, or ****$p < 0.0001$) was calculated using Student's t-test. n.s: not significant.

Supplementary Data 1

a, Gonadal WAT weights of *Mkl2* KO mice and their littermates. **b**, Brown adipose tissue (BAT) weights of *Mkl2* KO mice and their littermates. **c, d**, WAT of *Mkl2* KO mice and their littermates. Epididymal WAT (**c**) and mesenteric fat (**d**). **a, b**, Data are presented as box plots (WT: n=11, Ht: n=11, KO: n=6). Significance (*$p < 0.05$) was calculated using Dunnett's multiple comparison test. n.s: not significant.

Supplementary Data 2

a-d, Skeletal muscle weights of *Mkl2* KO mice and their littermates. Wt: Wild type, Ht: Heterozygous knockout, KO: Knockout. **e-h,** Tibialis anterior (**e**), soleus (**f**), plantaris (**g**) and extensor digitorum longus muscles (**h**) from *Mkl2* KO mouse and littermate. **a-d**, Data are presented as box plots (WT: n=11, Ht: n=11, KO: n=6). Significance (*$p < 0.05$ or **$p < 0.01$) was calculated using Dunnett's multiple comparison test.

Supplementary Data 3

a, Expression of Foxo1 target genes in inguinal WAT of *Mkl2* KO mice and their littermates. Data are mean ± s.d. (n=4). Significance (*$p < 0.05$) was calculated using Student's t-test.

Supplementary Data 4

a, b, Inhibitory effects of Mkl1 on the transcriptional activity of Foxo1, Foxo3 and Foxo4 using luciferase reporters with FoxO response elements in the normal state (**a**) or in the state of PI3K/AKT pathway suppressed by LY294002 treatment (**b**). Data are mean ± s.d. of n = 3 cultures per condition. Significance (****$p < 0.0001$) was calculated using Student's t-test.

Supplementary Data 5

a-d, Protein-protein interaction (PPI) between Foxo1 and Mkl1 (**a, b**) or Mkl2 (**c, d**) detected by split luciferase (NanoBiT). PPI was measured for all possible combinations (Lg: LgBiT tag, Sm: SmBiT tag, HT: Halotag). The relative PPI signal was calculated

based on the signal between the LgBiT tagged protein and the SmBiT-Halotag. **e**, Changes in the interaction of Foxo1 with Mkl1 or Mkl2 by adding CCG-1423 were measured in a different combination than shown in Figure 2f. Data are mean ± s.d. of n = 3 cultures per condition. Significance (*$p < 0.05$, **$p < 0.01$, ***$p < 0.001$, or ****$p < 0.0001$) was calculated using Student's t-test (**e**) or Dunnett's multiple comparison test (**a-d**). n.s: not significant.

Supplementary Data 6

a-b, Luciferase assay using a reporter with *Pparγ* responsive elements. Pparγ transcriptional activity was suppressed by a constitutively active mutant of Foxo1 (ADA), but restored by Mkl2 (**a**) and Mkl1 (**b**). Data are mean ± s.d. of n = 3 cultures per condition. Significance (**$p < 0.01$ or ****$p < 0.0001$) was calculated using Dunnett's multiple comparison test.

Supplementary Data 7

a, Oil red O staining of *Mkl1* knockdown 3T3-L1 cells at day 8 of differentiation. **b,** After staining, the dye was extracted with isopropanol and quantified by absorbance at 490 nm. **c**, mRNA expression of *Pparγ*, *Plin1* and *Hsl* at day 4, 7 and 10 after induction of differentiation of 3T3-L1 cells with or without *Mkl1* knockdown. The mRNA expression is shown as a relative change from the average expression of the control on day 4. **d**, Protein expression of *Pparγ*, *Plin1* and *Hsl* at day 4, 7 and 10 after induction of differentiation of 3T3-L1 cells with or without *Mkl1* knockdown. **e**, Subcellular localization of Mkl1 with Foxo1 or Foxo1(ADA) expression. The percentages of cells showing nuclear and cytoplasmic localization for Foxo1 and Mkl1, respectively, are shown below (C: cytoplasmic localization, N: nuclear localization). Data are mean ± s.d. of n = 3 cultures per condition. Significance (****$p < 0.0001$) was calculated using Dunnett's test for multiple comparisons.

Supplementary Data 8

a, **b**, Changes in localization of Foxo1 and Mkl1 (**a**) or Mkl2 (**b**) after addition of LY294002, a PI3K inhibitor. Changes in nuclear signal over time are shown on the right for two cells showing representative behavior. **c**, Changes in Mkl1 localization by treatment with or without leptomycin B.

Supplementary Data 9

Expression profiles of *atrogin-1*, *MuRF1*, *Foxo1*, *Foxo3*, *Foxo4*, *Mkl1* and *Mkl2* in the

gastrocnemius muscle of 8, 18, 22, 24, 26 and 28 month old mice. These data are from a re-analysis of the GEO data set (GEO accession number: GSE145480). Significance (*p < 0.05, **p < 0.01, ***p < 0.001, or ****p < 0.0001) was calculated using Dunnett's test for multiple comparisons. n.s: not significant.

Supplementary Data 10

a, Changes in the expression of atrogenes, *Foxo1*, *Foxo3*, *Foxo4*, *Mkl1* and *Mkl2* in the left or right gastrocnemius muscle of mice with sciatic nerve denervation of the right hindlimb. Day is the number of days after sciatic nerve denervation. **b**, Inverse correlation of *Mkl1* and atrogene expression levels in the gastrocnemius muscle of mice with right hindlimb sciatic nerve denervation. Each point represents relative gene expression in either the left or right mouse gastrocnemius muscle. Relative gene expression was calculated based on the average expression in the left leg before sciatic nerve denervation (day 0). Data are mean ± s.d. (n=5). Significance (**p < 0.01, ***p < 0.001, or ****p < 0.0001) was calculated using Student's t-test. n.s: not significant.

Supplementary Data 11

a, Changes in the expression of atrogenes, *Foxo1*, *Foxo3*, *Foxo4*, *Mkl1* and *Mkl2* in the gastrocnemius muscle of 9-week-old C57BL/6J male mice fasted for 24 hours. **b**, Inverse correlation of *Mkl1* and atrogene expression levels in the gastrocnemius muscle of mice fasted for 24 hours. Each point represents the relative gene expression in the gastrocnemius muscle of one mouse. Relative gene expression was calculated based on the average expression of fed mice. Data are mean ± s.d. (n=4). Significance (*p < 0.05, **p < 0.01, ***p < 0.001, or ****p < 0.0001) was calculated using Student's t-test. n.s: not significant.

Supplementary Data 12

Changes in the expression of atrogenes, *Foxo1*, *Foxo3*, *Foxo4*, *Mkl1* and *Mkl2* in the gastrocnemius muscle of C57BL/6J mice 16 hours after intraperitoneal administration of dexamethasone sodium phosphate. Data are mean ± s.d. (n=7-8). Significance (*p < 0.05 or ****p < 0.0001) was calculated using Student's t-test. n.s: not significant.

Supplementary Data 13

Changes in the expression of atrogenes, *Foxo1*, *Foxo3*, *Foxo4*, *Mkl1* and *Mkl2* in mice with cancer cachexia. These data are from a re-analysis of the GEO dataset (GEO accession number: GSE65936). Data are mean ± s.d. (n=3). Significance (*p < 0.05, **p

< 0.01, or ***p < 0.001) was calculated using Student's t-test. n.s: not significant.

Supplementary Data 14

a, *Mkl1* expression in C2C12-derived myotubes by hydrocortisone or dexamethasone treatment. **b,** *Mkl1* expression in C2C12-derived myotubes when *Foxo1* or *Foxo3* is expressed by adenovirus or when Foxo1/3/4 is activated by the PI3K inhibitor LY294002. Data are mean ± s.d. of n = 3 cultures per condition. Significance (**p < 0.01) was calculated using Dunnett's test for multiple comparisons. n.s: not significant.

Supplementary Data 15

a, Changes in Foxo3 binding to FoxO binding sites on genomic regions near *atrogin-1* (**a**) or *MuRF1* (**b**) due to *Mkl1* or *Mkl2* expression as measured by chromatin immunoprecipitation (ChIP-qPCR).

Supplementary Data 16

a, b, Inhibitory effect of *Mkl1* or *Mkl2* on the transcriptional activity of the glucocorticoid receptor (GR) using luciferase reporters with GR response elements in the absence (**a**) or presence (**b**) of dexamethasone. **c, d** Protein-protein interaction (PPI) between GR and Mkl1 (**c**) or Mkl2 (**d**) detected by split luciferase (NanoBiT). The relative PPI signal was calculated based on the signal between the LgBiT-tagged GR and the SmBiT-Halotag (Lg: LgBiT tag, Sm: SmBiT tag, HT: Halotag). Data are mean ± s.d. of n = 3 cultures per condition. Significance (**p < 0.01 or ****p < 0.0001) was calculated using Dunnett's test for multiple comparisons.

Supplementary Data 17

a, b, Verification of the knockdown efficiency of *Mkl1* (**a**) and *Mkl2* (**b**) in C2C12-derived myotubes. Knockdown was achieved by infection with adenoviruses expressing artificial microRNAs (miRNAs) against *Mkl1* or *Mkl2*. Data are mean ± s.d. of n = 3 cultures per condition. Significance (****p < 0.0001) was calculated using Dunnett's multiple comparison test.

Supplementary Data 18

a, Changes in AkaLuc expression over time in mice treated systemically with MyoAAV.2A(Mhck7-AkaLuc-eGFP). Bioluminescence was measured using the IVIS LuminaII imaging system. **b**, eGFP expression observed in each muscle and heart of mice treated systemically with MyoAAV.2A (Mhck7-AkaLuc-eGFP).

Supplementary Data 19

a, b, Heart weight (**a**) and morphology (**b**) of mice treated systemically with MyoAAV.2A (Mhck7-*Mkl1*) at different viral concentrations. Data were presented in a box plot (n=3-4). Significance (****$p < 0.0001$) was calculated using Dunnett's test for multiple comparisons. n.s: not significant.

Supplementary Data 20

Comparison of atrogene expression in the gastrocnemius muscle of mice expressing *Mkl1* in the muscle by MyoAAV.2A and fasted for 24 hours. Data are mean ± s.d. (n=3-4). Significance (*$p < 0.05$ or **$p < 0.01$) was calculated using Student's t-test. n.s: not significant.

Supplementary Data 21

Schematic diagram showing the effects of Mkl1 and Mkl2 on the GR/FoxO pathway, which regulates the progression of muscle atrophy. Exercise activates *Mkl1/2* through nuclear translocation of Mkl2 and increased expression of *Mkl1/2*. However, *Mkl1* expression decreases in response to the onset of muscle atrophy. GR: Glucocorticoid receptor.

Supplementary Movie1

Time-lapse imaging of Foxo1-eGFP and Mkl2-mCherry localization in 3T3-L1 preadipocytes after addition of the PI3K inhibitor wortmannin. The green channel (left) represents Foxo1-eGFP. The red channel (center) represents Mkl2-mCherry. The merged image is shown on the right. This movie corresponds to Fig. 3h.

Supplementary Movie2

Nuclear accumulation of Mkl2-eGFP during contraction of C2C12-derived myotubes 3 hours after initiation of electrical pulse stimulation (EPS). Adenovirus was used to express Mkl2-eGFP in myotubes and EPS was applied at a frequency of 1 Hz. This movie corresponds to the right figures in Fig. 6e.

REFERENCES

1 Calissi, G., Lam, E. W. & Link, W. Therapeutic strategies targeting FOXO transcription factors. *Nat Rev Drug Discov* **20**, 21-38 (2021). https://doi.org:10.1038/s41573-020-0088-2

2 Eijkelenboom, A. & Burgering, B. M. FOXOs: signalling integrators for homeostasis maintenance. *Nat Rev Mol Cell Biol* **14**, 83-97 (2013). https://doi.org:10.1038/nrm3507

3 Kenyon, C., Chang, J., Gensch, E., Rudner, A. & Tabtiang, R. A C. elegans mutant that lives twice as long as wild type. *Nature* **366**, 461-464 (1993). https://doi.org:DOI 10.1038/366461a0

4 Sasako, T. *et al.* Deletion of skeletal muscle Akt1/2 causes osteosarcopenia and reduces lifespan in mice. *Nat Commun* **13**, 5655 (2022). https://doi.org:10.1038/s41467-022-33008-2

5 Hosooka, T. *et al.* The PDK1-FoxO1 signaling in adipocytes controls systemic insulin sensitivity through the 5-lipoxygenase-leukotriene B(4) axis. *Proc Natl Acad Sci U S A* **117**, 11674-11684 (2020). https://doi.org:10.1073/pnas.1921015117

6 Brunet, A. *et al.* Akt promotes cell survival by phosphorylating and inhibiting a Forkhead transcription factor. *Cell* **96**, 857-868 (1999). https://doi.org:10.1016/s0092-8674(00)80595-4

7 Ou, M. Y., Zhang, H., Tan, P. C., Zhou, S. B. & Li, Q. F. Adipose tissue aging: mechanisms and therapeutic implications. *Cell Death Dis* **13**, 300 (2022). https://doi.org:10.1038/s41419-022-04752-6

8 Tchkonia, T. *et al.* Fat tissue, aging, and cellular senescence. *Aging Cell* **9**, 667-684 (2010). https://doi.org:10.1111/j.1474-9726.2010.00608.x

9 Armoni, M. *et al.* FOXO1 represses peroxisome proliferator-activated receptor-gamma1 and -gamma2 gene promoters in primary adipocytes. A novel paradigm to increase insulin sensitivity. *J Biol Chem* **281**, 19881-19891 (2006). https://doi.org:10.1074/jbc.M600320200

10 Dowell, P., Otto, T. C., Adi, S. & Lane, M. D. Convergence of peroxisome proliferator-activated receptor gamma and Foxo1 signaling pathways. *J Biol Chem* **278**, 45485-45491 (2003). https://doi.org:10.1074/jbc.M309069200

11 Fan, W. *et al.* FOXO1 transrepresses peroxisome proliferator-activated receptor gamma transactivation, coordinating an insulin-induced feed-forward response in adipocytes. *J Biol Chem* **284**, 12188-12197 (2009). https://doi.org:10.1074/jbc.M808915200

12 Nakae, J. *et al.* The forkhead transcription factor Foxo1 regulates adipocyte differentiation. *Dev Cell* **4**, 119-129 (2003). https://doi.org:10.1016/s1534-

5807(02)00401-x

13 Sandri, M. *et al.* Foxo transcription factors induce the atrophy-related ubiquitin ligase atrogin-1 and cause skeletal muscle atrophy. *Cell* **117**, 399-412 (2004). https://doi.org:10.1016/s0092-8674(04)00400-3

14 Stitt, T. N. *et al.* The IGF-1/PI3K/Akt pathway prevents expression of muscle atrophy-induced ubiquitin ligases by inhibiting FOXO transcription factors. *Mol Cell* **14**, 395-403 (2004). https://doi.org:10.1016/s1097-2765(04)00211-4

15 Lecker, S. H. *et al.* Multiple types of skeletal muscle atrophy involve a common program of changes in gene expression. *FASEB J* **18**, 39-51 (2004). https://doi.org:10.1096/fj.03-0610com

16 Sartori, R., Romanello, V. & Sandri, M. Mechanisms of muscle atrophy and hypertrophy: implications in health and disease. *Nature Communications* **12** (2021). https://doi.org:10.1038/s41467-020-20123-1

17 Milan, G. *et al.* Regulation of autophagy and the ubiquitin-proteasome system by the FoxO transcriptional network during muscle atrophy. *Nat Commun* **6**, 6670 (2015). https://doi.org:10.1038/ncomms7670

18 Kang, S. H. *et al.* Forkhead box O3 plays a role in skeletal muscle atrophy through expression of E3 ubiquitin ligases MuRF-1 and atrogin-1 in Cushing's syndrome. *Am J Physiol Endocrinol Metab* **312**, E495-E507 (2017). https://doi.org:10.1152/ajpendo.00389.2016

19 Shimizu, N. *et al.* Crosstalk between glucocorticoid receptor and nutritional sensor mTOR in skeletal muscle. *Cell Metab* **13**, 170-182 (2011). https://doi.org:10.1016/j.cmet.2011.01.001

20 Waddell, D. S. *et al.* The glucocorticoid receptor and FOXO1 synergistically activate the skeletal muscle atrophy-associated MuRF1 gene. *Am J Physiol Endocrinol Metab* **295**, E785-797 (2008). https://doi.org:10.1152/ajpendo.00646.2007

21 Graham, Z. A. *et al.* Mechanisms of exercise as a preventative measure to muscle wasting. *Am J Physiol Cell Physiol* **321**, C40-C57 (2021). https://doi.org:10.1152/ajpcell.00056.2021

22 Ruas, J. L. *et al.* A PGC-1alpha isoform induced by resistance training regulates skeletal muscle hypertrophy. *Cell* **151**, 1319-1331 (2012). https://doi.org:10.1016/j.cell.2012.10.050

23 Short, K. R. *et al.* Impact of aerobic exercise training on age-related changes in insulin sensitivity and muscle oxidative capacity. *Diabetes* **52**, 1888-1896 (2003). https://doi.org:10.2337/diabetes.52.8.1888

24 Brault, J. J., Jespersen, J. G. & Goldberg, A. L. Peroxisome proliferator-activated

receptor gamma coactivator 1alpha or 1beta overexpression inhibits muscle protein degradation, induction of ubiquitin ligases, and disuse atrophy. *J Biol Chem* **285**, 19460-19471 (2010). https://doi.org:10.1074/jbc.M110.113092

25 Sandri, M. *et al.* PGC-1alpha protects skeletal muscle from atrophy by suppressing FoxO3 action and atrophy-specific gene transcription. *Proc Natl Acad Sci U S A* **103**, 16260-16265 (2006). https://doi.org:10.1073/pnas.0607795103

26 Geng, T., Li, P., Yin, X. & Yan, Z. PGC-1alpha promotes nitric oxide antioxidant defenses and inhibits FOXO signaling against cardiac cachexia in mice. *Am J Pathol* **178**, 1738-1748 (2011). https://doi.org:10.1016/j.ajpath.2011.01.005

27 Olson, E. N. & Nordheim, A. Linking actin dynamics and gene transcription to drive cellular motile functions. *Nat Rev Mol Cell Biol* **11**, 353-365 (2010). https://doi.org:10.1038/nrm2890

28 Parmacek, M. S. Myocardin-related transcription factors: critical coactivators regulating cardiovascular development and adaptation. *Circ Res* **100**, 633-644 (2007). https://doi.org:10.1161/01.RES.0000259563.61091.e8

29 Li, J. *et al.* Myocardin-related transcription factor B is required in cardiac neural crest for smooth muscle differentiation and cardiovascular development. *P Natl Acad Sci USA* **102**, 8916-8921 (2005). https://doi.org:10.1073/pnas.0503741102

30 Oh, J., Richardson, J. A. & Olson, E. N. Requirement of myocardin-related transcription factor-B for remodeling of branchial arch arteries and smooth muscle differentiation. *Proc Natl Acad Sci U S A* **102**, 15122-15127 (2005). https://doi.org:10.1073/pnas.0507346102

31 Capell, B. C. & Collins, F. S. Human laminopathies: nuclei gone genetically awry. *Nat Rev Genet* **7**, 940-952 (2006). https://doi.org:10.1038/nrg1906

32 Schreiber, K. H. & Kennedy, B. K. When lamins go bad: nuclear structure and disease. *Cell* **152**, 1365-1375 (2013). https://doi.org:10.1016/j.cell.2013.02.015

33 Ho, C. Y., Jaalouk, D. E., Vartiainen, M. K. & Lammerding, J. Lamin A/C and emerin regulate MKL1-SRF activity by modulating actin dynamics. *Nature* **497**, 507-511 (2013). https://doi.org:10.1038/nature12105

34 Auguste, G. *et al.* Suppression of Activated FOXO Transcription Factors in the Heart Prolongs Survival in a Mouse Model of Laminopathies. *Circ Res* **122**, 678-692 (2018). https://doi.org:10.1161/CIRCRESAHA.117.312052

35 Hayashi, K., Watanabe, B., Nakagawa, Y., Minami, S. & Morita, T. RPEL proteins are the molecular targets for CCG-1423, an inhibitor of Rho signaling. *PLoS One* **9**, e89016 (2014). https://doi.org:10.1371/journal.pone.0089016

36 Borsch, A. *et al.* Molecular and phenotypic analysis of rodent models reveals conserved

and species-specific modulators of human sarcopenia. *Commun Biol* **4**, 194 (2021). https://doi.org:10.1038/s42003-021-01723-z

37 Tseng, Y. C. *et al.* Preclinical Investigation of the Novel Histone Deacetylase Inhibitor AR-42 in the Treatment of Cancer-Induced Cachexia. *J Natl Cancer Inst* **107**, djv274 (2015). https://doi.org:10.1093/jnci/djv274

38 Oki, S. *et al.* ChIP-Atlas: a data-mining suite powered by full integration of public ChIP-seq data. *EMBO Rep* **19** (2018). https://doi.org:10.15252/embr.201846255

39 Tabebordbar, M. *et al.* Directed evolution of a family of AAV capsid variants enabling potent muscle-directed gene delivery across species. *Cell* **184**, 4919-4938 e4922 (2021). https://doi.org:10.1016/j.cell.2021.08.028

40 Lamon, S., Wallace, M. A., Leger, B. & Russell, A. P. Regulation of STARS and its downstream targets suggest a novel pathway involved in human skeletal muscle hypertrophy and atrophy. *J Physiol* **587**, 1795-1803 (2009). https://doi.org:10.1113/jphysiol.2009.168674

41 Nobusue, H. *et al.* Regulation of MKL1 via actin cytoskeleton dynamics drives adipocyte differentiation. *Nat Commun* **5**, 3368 (2014). https://doi.org:10.1038/ncomms4368

42 McDonald, M. E. *et al.* Myocardin-related transcription factor A regulates conversion of progenitors to beige adipocytes. *Cell* **160**, 105-118 (2015). https://doi.org:10.1016/j.cell.2014.12.005

43 Zou, P. *et al.* Targeting FoxO1 with AS1842856 suppresses adipogenesis. *Cell Cycle* **13**, 3759-3767 (2014). https://doi.org:10.4161/15384101.2014.965977

44 Ortega-Molina, A. *et al.* Pten positively regulates brown adipose function, energy expenditure, and longevity. *Cell Metab* **15**, 382-394 (2012). https://doi.org:10.1016/j.cmet.2012.02.001

45 Li, S. *et al.* Requirement for serum response factor for skeletal muscle growth and maturation revealed by tissue-specific gene deletion in mice. *Proc Natl Acad Sci U S A* **102**, 1082-1087 (2005). https://doi.org:10.1073/pnas.0409103102

46 Xia, P. *et al.* Doxorubicin induces cardiomyocyte apoptosis and atrophy through cyclin-dependent kinase 2-mediated activation of forkhead box O1. *J Biol Chem* **295**, 4265-4276 (2020). https://doi.org:10.1074/jbc.RA119.011571

47 Chan, K. Y. *et al.* Engineered AAVs for efficient noninvasive gene delivery to the central and peripheral nervous systems. *Nat Neurosci* **20**, 1172-1179 (2017). https://doi.org:10.1038/nn.4593

Fig. 1

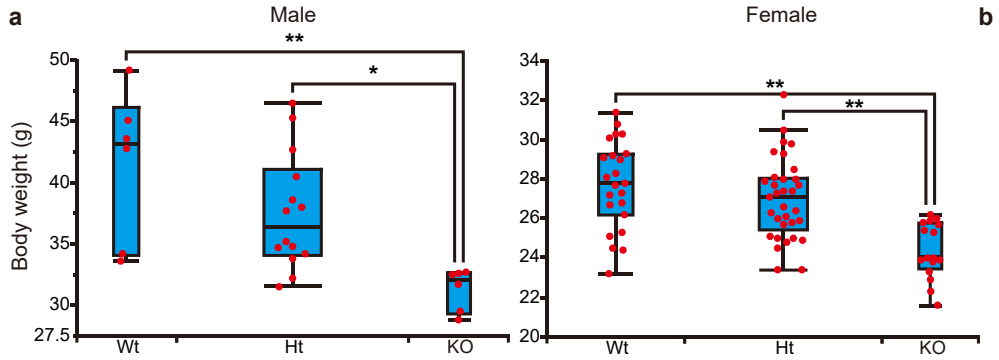

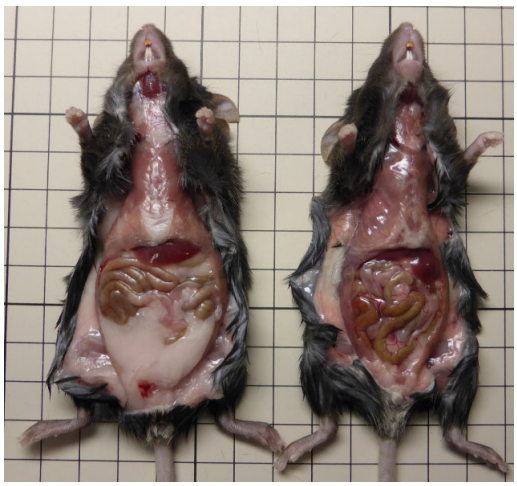

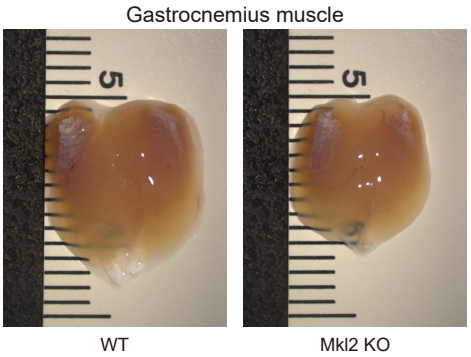

g Top 10 TFs predicted by upstream analysis

TF	Predicted Activation State	Activation z-score	p-value of overlap
Mef2c	Inhibited	-4.355	5.97E-13
Myod1	Inhibited	-3.839	3.42E-11
Foxo1	Activated	2.226	5.43E-10
Trp53	Inhibited	-3.988	5.49E-10
Ets1	Activated	2.701	5.39E-09
Srf	Inhibited	-2.674	6.47E-09
Med13	Inhibited	-2.121	2.34E-07
Sirt1	Inhibited	-2.31	3.60E-07
Tbx5	Inhibited	-3.053	3.33E-06
Prdm1	Inhibited	-3.41	7.44E-06

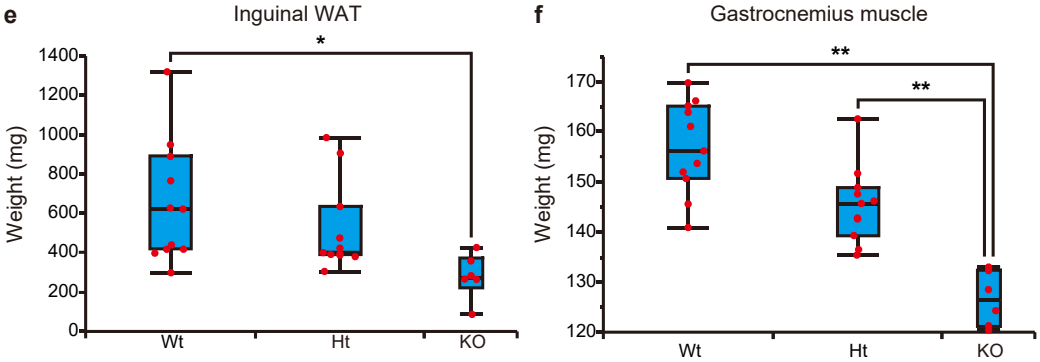

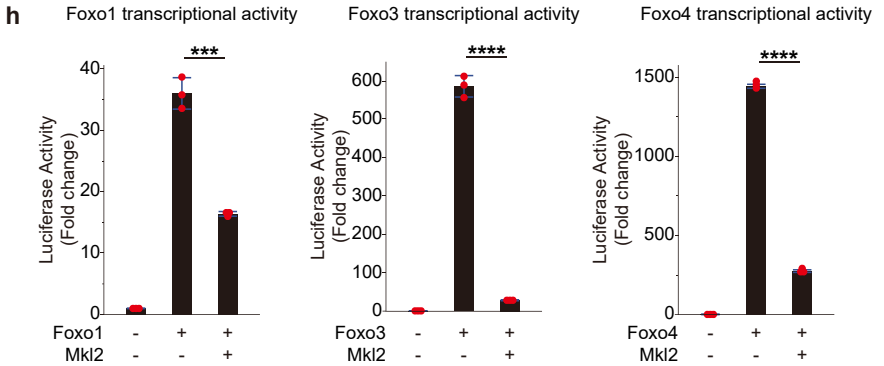

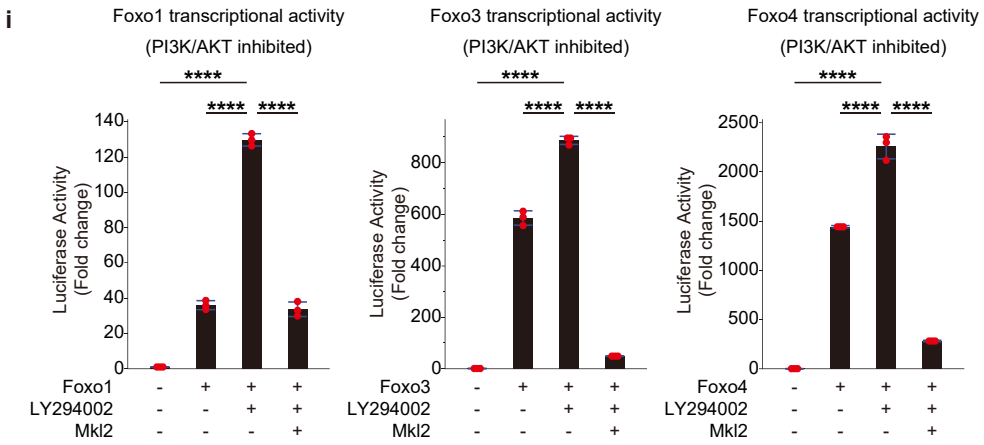

Fig.2

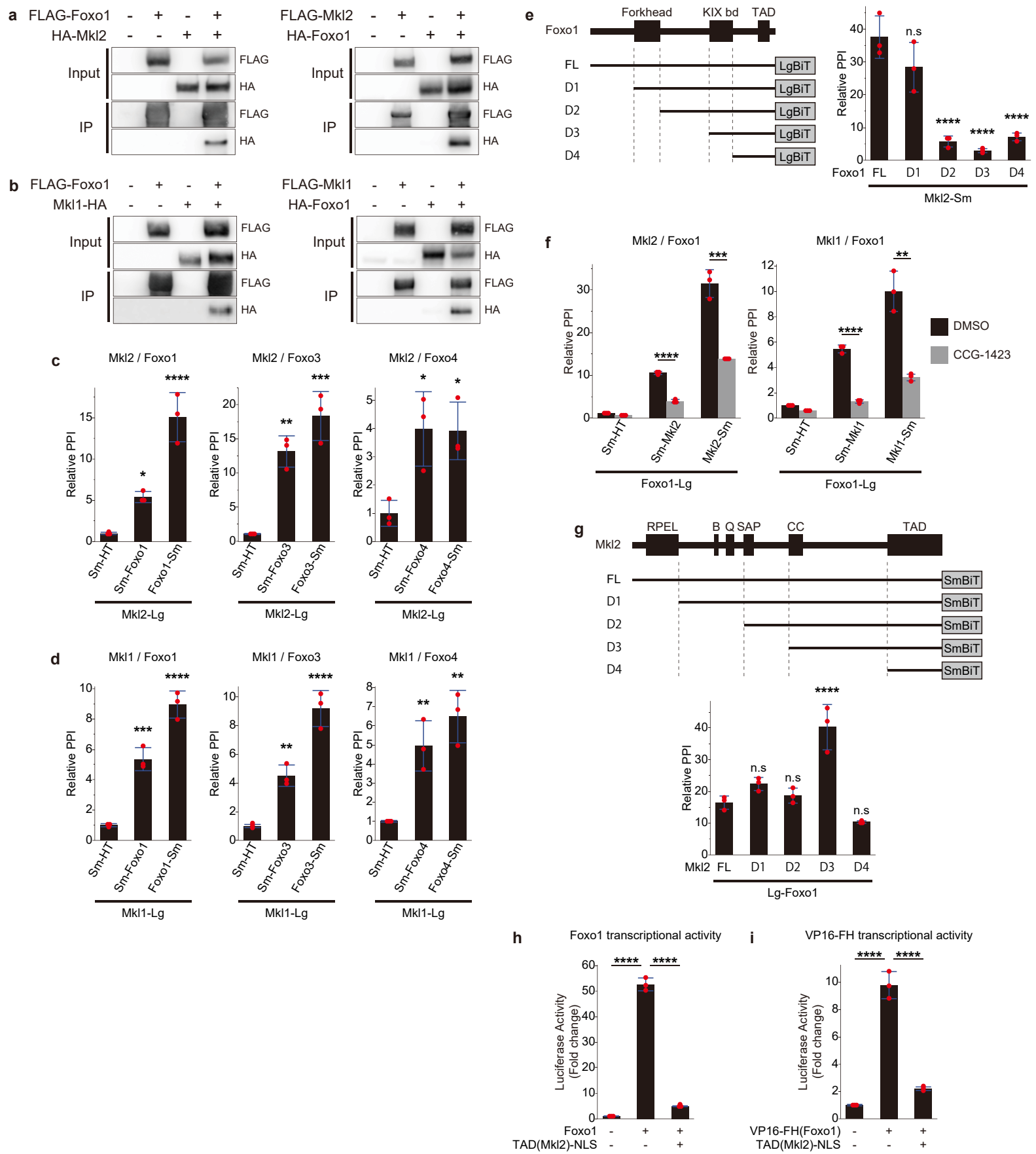
a
FLAG-Foxo1 - + - +
HA-Mkl2 - - + +
Input
IP
FLAG
HA
FLAG-Mkl2 - + - +
HA-Foxo1 - - + +
b
FLAG-Foxo1 - + - +
Mkl1-HA - - + +
FLAG-Mkl1 - + - +
HA-Foxo1 - - + +
c
Mkl2 / Foxo1
Mkl2 / Foxo3
Mkl2 / Foxo4
Relative PPI
Sm-HT
Sm-Foxo1
Foxo1-Sm
Sm-Foxo3
Foxo3-Sm
Sm-Foxo4
Foxo4-Sm
Mkl2-Lg
d
Mkl1 / Foxo1
Mkl1 / Foxo3
Mkl1 / Foxo4
Mkl1-Lg
e
Forkhead
KIX bd
TAD
Foxo1
FL
D1
D2
D3
D4
LgBiT
n.s
Mkl2-Sm
f
Mkl2 / Foxo1
Mkl1 / Foxo1
DMSO
CCG-1423
Sm-Mkl2
Mkl2-Sm
Sm-Mkl1
Mkl1-Sm
Foxo1-Lg
g
RPEL
B Q SAP
CC
TAD
Mkl2
SmBiT
Lg-Foxo1
h
Foxo1 transcriptional activity
Luciferase Activity (Fold change)
TAD(Mkl2)-NLS
i
VP16-FH transcriptional activity
VP16-FH(Foxo1)

Fig. 3

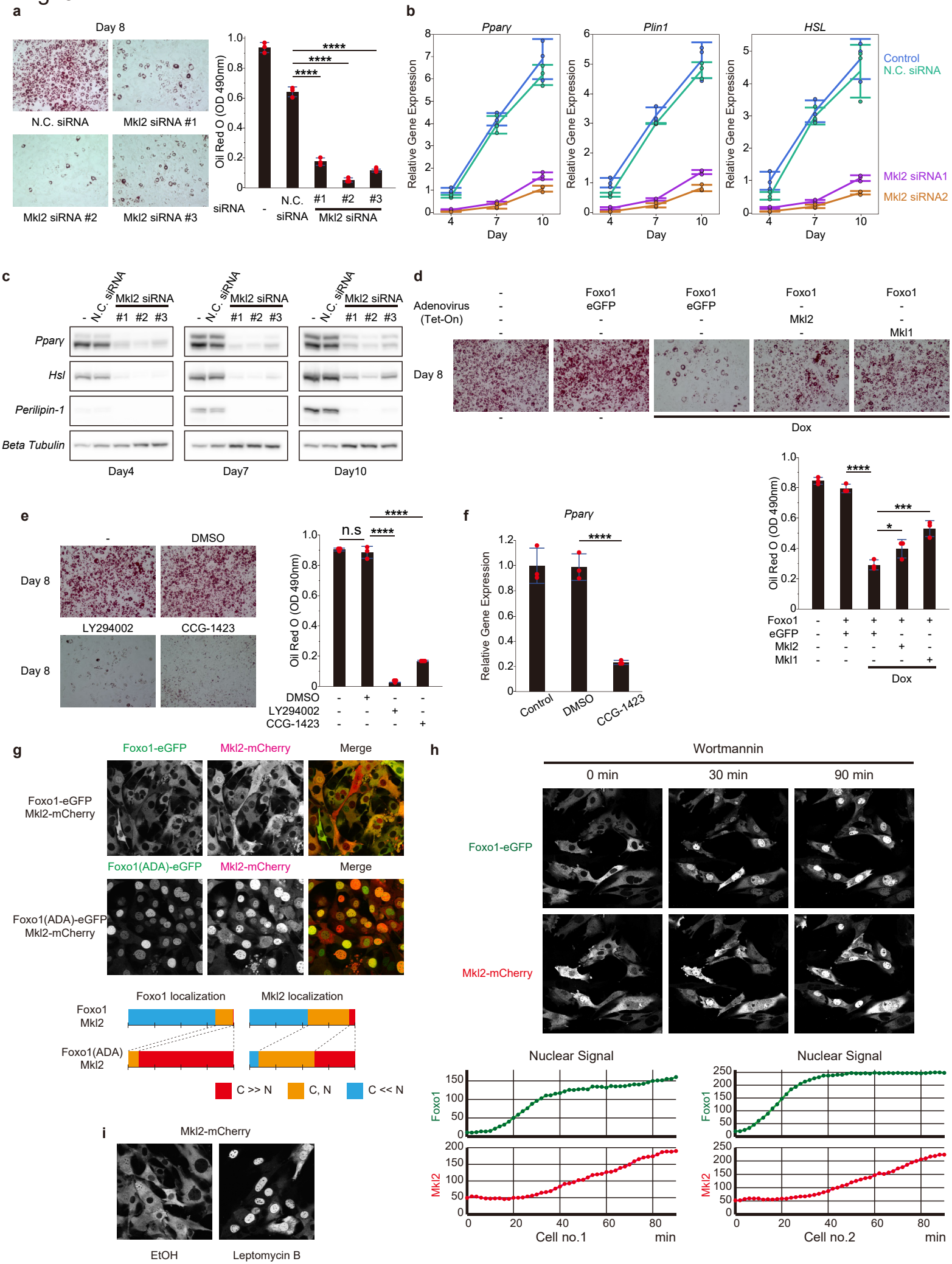
a
Day 8
N.C. siRNA
Mkl2 siRNA #1
Mkl2 siRNA #2
Mkl2 siRNA #3
Oil Red O (OD 490nm)
siRNA
N.C. siRNA
Mkl2 siRNA
#1
#2
#3
****
b
Ppar γ
Plin1
HSL
Relative Gene Expression
Day
Control
N.C. siRNA
Mkl2 siRNA1
Mkl2 siRNA2
c
N.C. siRNA
Mkl2 siRNA
Ppar γ
Hsl
Perilipin-1
Beta Tubulin
Day4
Day7
Day10
d
Adenovirus (Tet-On)
Foxo1
eGFP
Mkl2
Mkl1
Day 8
Dox
Oil Red O (OD 490nm)
Foxo1
eGFP
Mkl2
Mkl1
***
*
e
DMSO
LY294002
CCG-1423
Day 8
n.s
Oil Red O (OD 490nm)
DMSO
LY294002
CCG-1423
f
Ppar γ
Relative Gene Expression
Control
DMSO
CCG-1423
g
Foxo1-eGFP
Mkl2-mCherry
Merge
Foxo1(ADA)-eGFP
Foxo1 localization
Mkl2 localization
Foxo1
Mkl2
Foxo1(ADA)
C >> N
C, N
C << N
h
Wortmannin
0 min
30 min
90 min
Foxo1-eGFP
Mkl2-mCherry
Nuclear Signal
Foxo1
Mkl2
Cell no.1
Cell no.2
min
i
Mkl2-mCherry
EtOH
Leptomycin B

Fig. 4

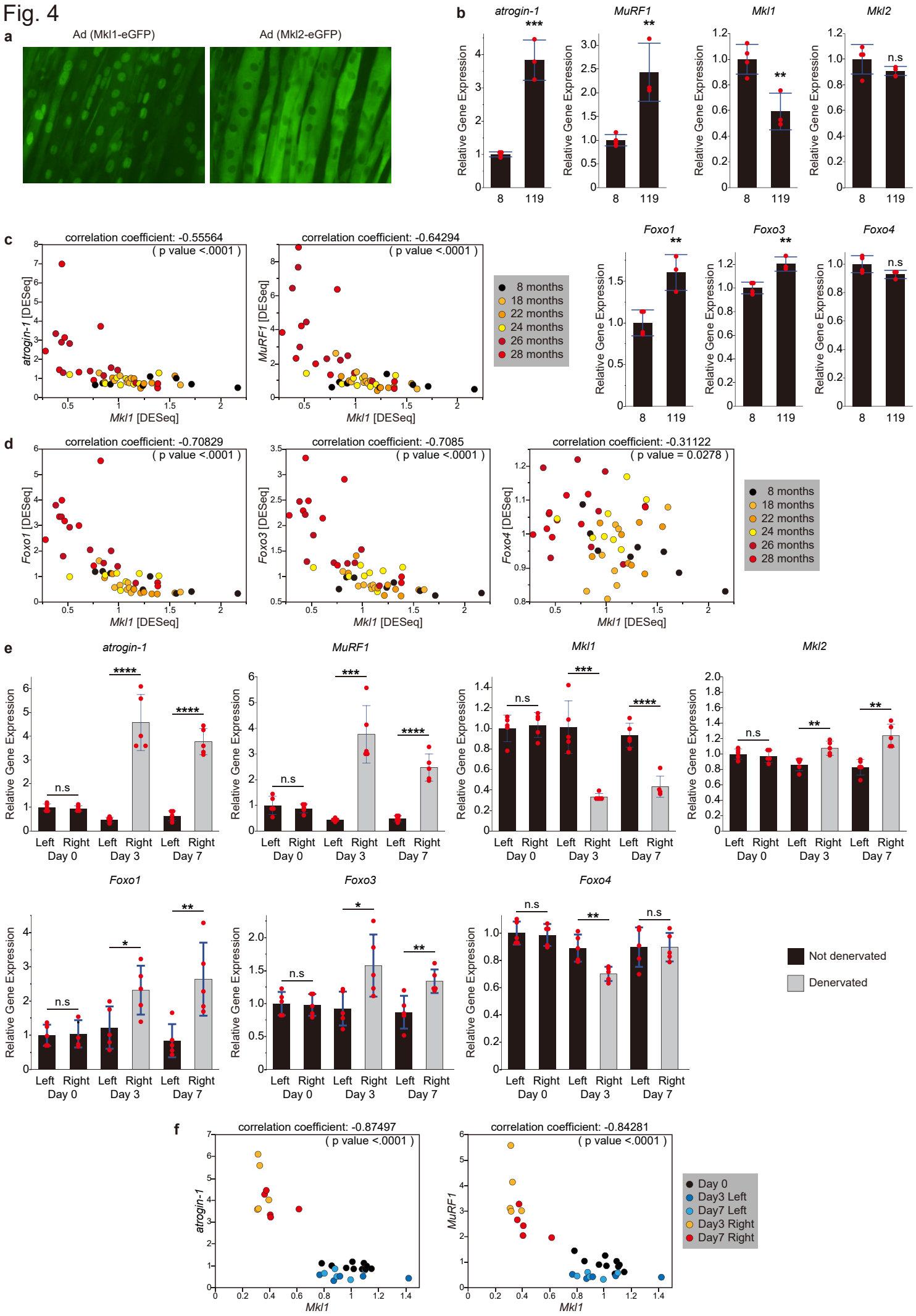
a
Ad (Mkl1-eGFP)
Ad (Mkl2-eGFP)
b
atrogin-1
MuRF1
Mkl1
Mkl2
Relative Gene Expression
8
119
n.s
c
correlation coefficient: -0.55564
(p value <.0001)
atrogin-1 [DESeq]
Mkl1 [DESeq]
correlation coefficient: -0.64294
(p value <.0001)
MuRF1 [DESeq]
8 months
18 months
22 months
24 months
26 months
28 months
Foxo1
Foxo3
Foxo4
d
correlation coefficient: -0.70829
(p value <.0001)
Foxo1 [DESeq]
correlation coefficient: -0.7085
(p value <.0001)
Foxo3 [DESeq]
correlation coefficient: -0.31122
(p value = 0.0278)
Foxo4 [DESeq]
e
Left
Right
Day 0
Day 3
Day 7
Not denervated
Denervated
f
correlation coefficient: -0.87497
(p value <.0001)
correlation coefficient: -0.84281
(p value <.0001)
Day 0
Day3 Left
Day7 Left
Day3 Right
Day7 Right

Fig. 5

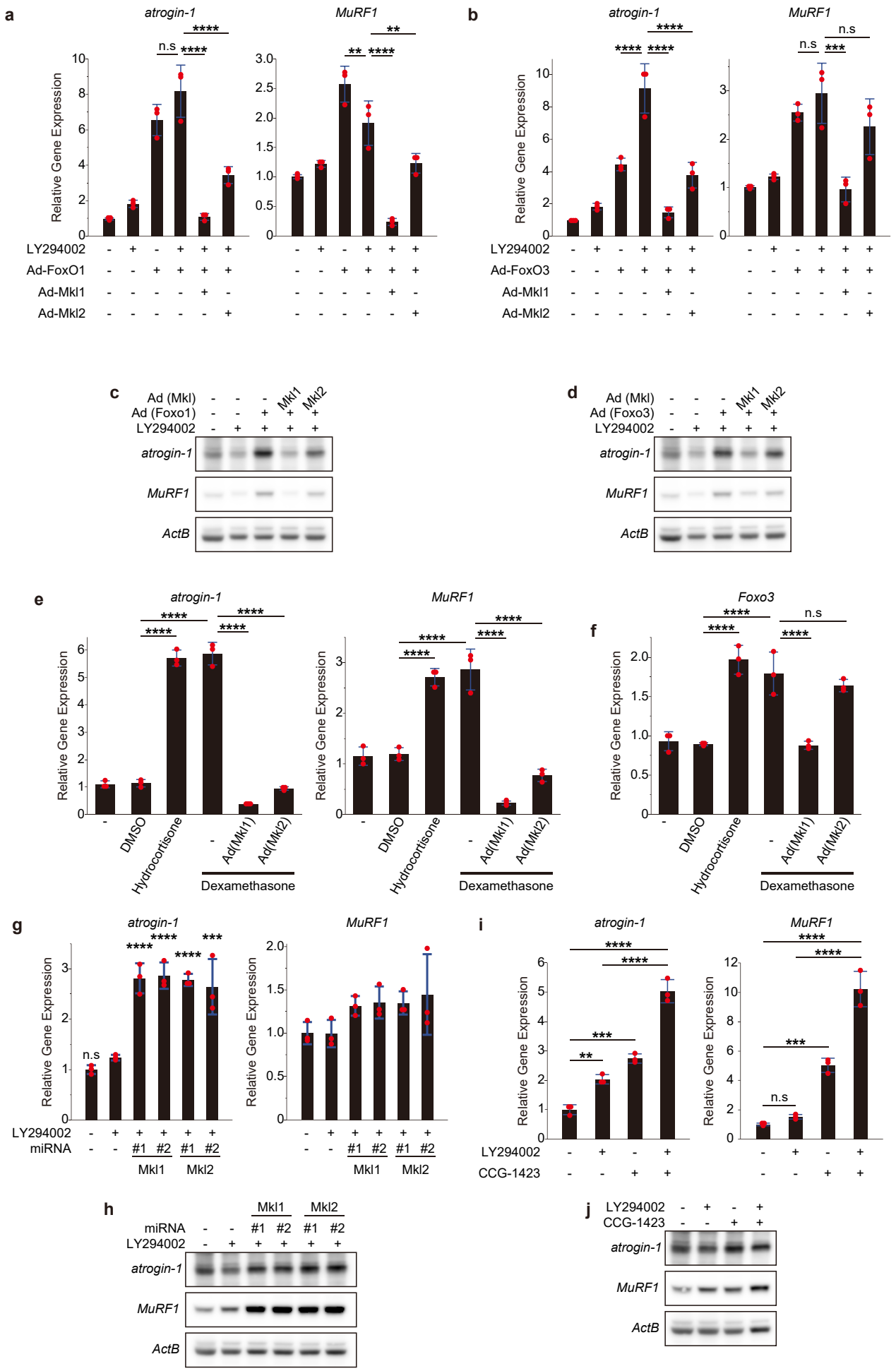
a
atrogin-1
MuRF1
Relative Gene Expression
LY294002
Ad-FoxO1
Ad-Mkl1
Ad-Mkl2
b
atrogin-1
MuRF1
Relative Gene Expression
LY294002
Ad-FoxO3
Ad-Mkl1
Ad-Mkl2
c
Ad (Mkl)
Ad (Foxo1)
LY294002
Mkl1
Mkl2
atrogin-1
MuRF1
ActB
d
Ad (Mkl)
Ad (Foxo3)
LY294002
Mkl1
Mkl2
atrogin-1
MuRF1
ActB
e
atrogin-1
MuRF1
Relative Gene Expression
DMSO
Hydrocortisone
Ad(Mkl1)
Ad(Mkl2)
Dexamethasone
f
Foxo3
Relative Gene Expression
DMSO
Hydrocortisone
Ad(Mkl1)
Ad(Mkl2)
Dexamethasone
g
atrogin-1
MuRF1
Relative Gene Expression
LY294002
miRNA
#1
#2
Mkl1
Mkl2
i
atrogin-1
MuRF1
Relative Gene Expression
LY294002
CCG-1423
h
Mkl1
Mkl2
miRNA
LY294002
atrogin-1
MuRF1
ActB
j
LY294002
CCG-1423
atrogin-1
MuRF1
ActB

Fig. 6

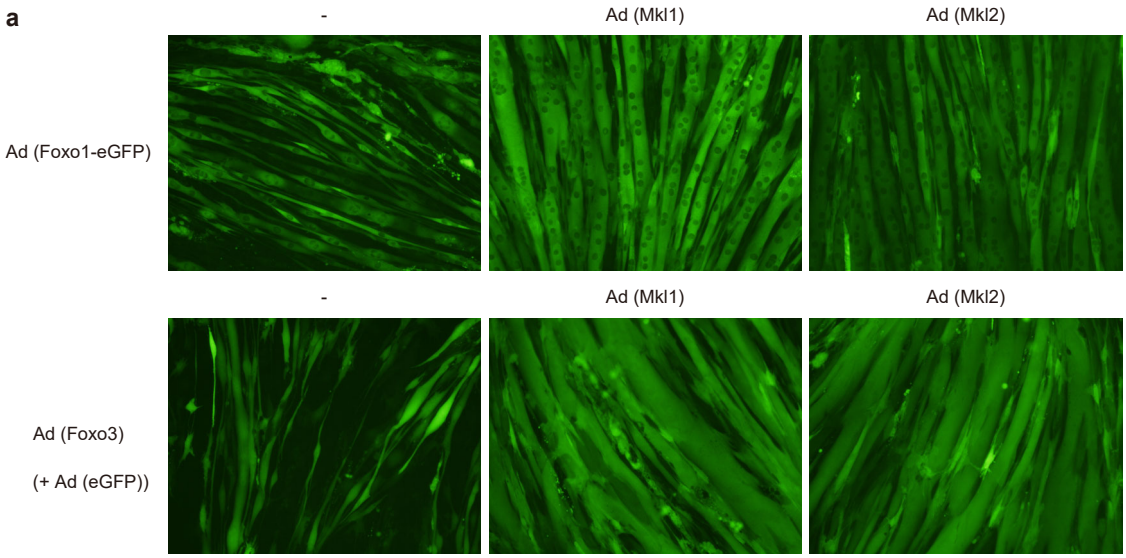
a
-
Ad (Mkl1)
Ad (Mkl2)
Ad (Foxo1-eGFP)
-
Ad (Mkl1)
Ad (Mkl2)
Ad (Foxo3)
(+ Ad (eGFP))

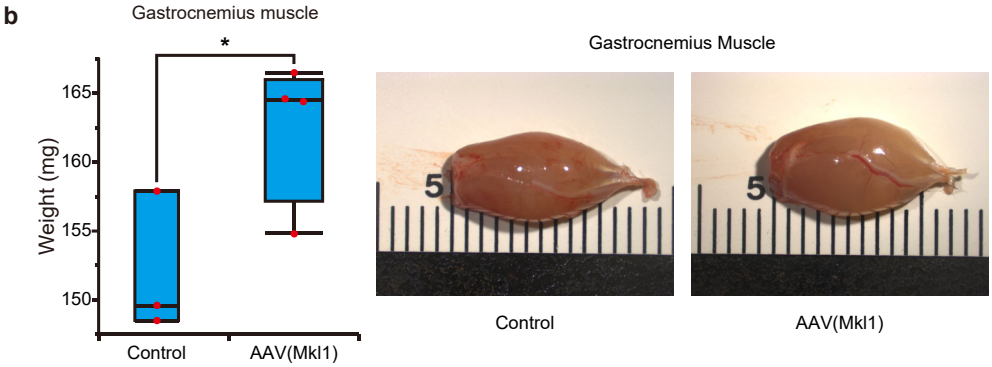
b
Gastrocnemius muscle
*
Weight (mg)
165
160
155
150
Control
AAV(Mkl1)
Gastrocnemius Muscle
5
5
Control
AAV(Mkl1)

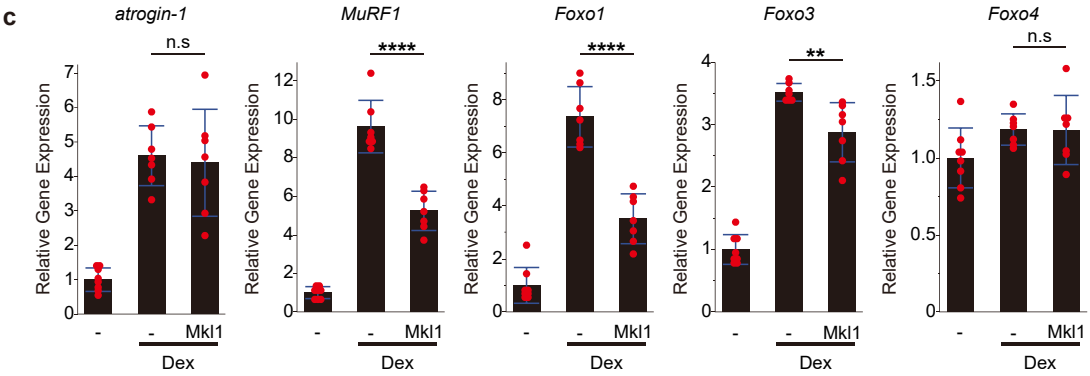
c
atrogin-1
n.s
MuRF1
****
Foxo1
****
Foxo3
**
Foxo4
n.s
Relative Gene Expression
-
-
Mkl1
Dex

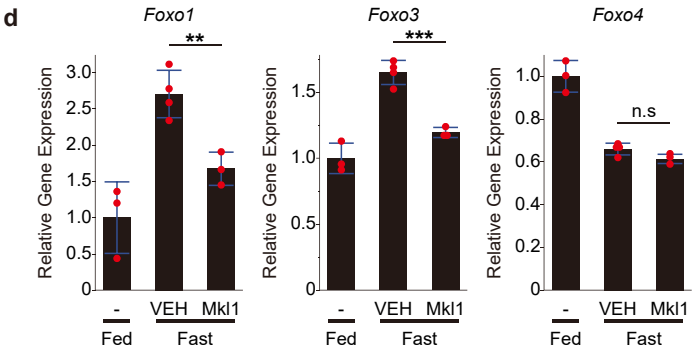
d
Foxo1
**
Foxo3
***
Foxo4
n.s
Relative Gene Expression
-
VEH
Mkl1
Fed
Fast

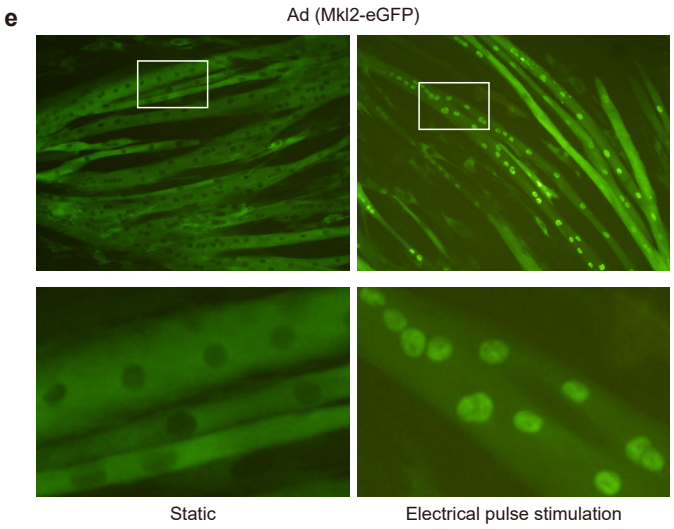
e
Ad (Mkl2-eGFP)
Static
Electrical pulse stimulation

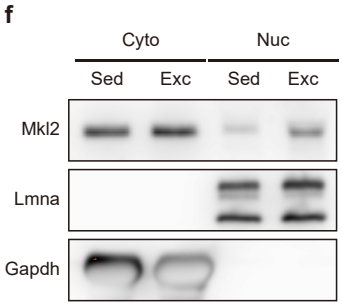
f
Cyto
Nuc
Sed
Exc
Sed
Exc
Mkl2
Lmna
Gapdh

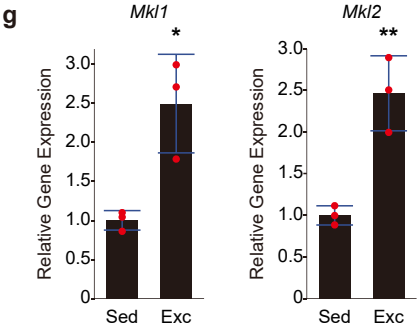
g
Mkl1
*
Mkl2
**
Relative Gene Expression
Sed
Exc

Supplementary Data 1

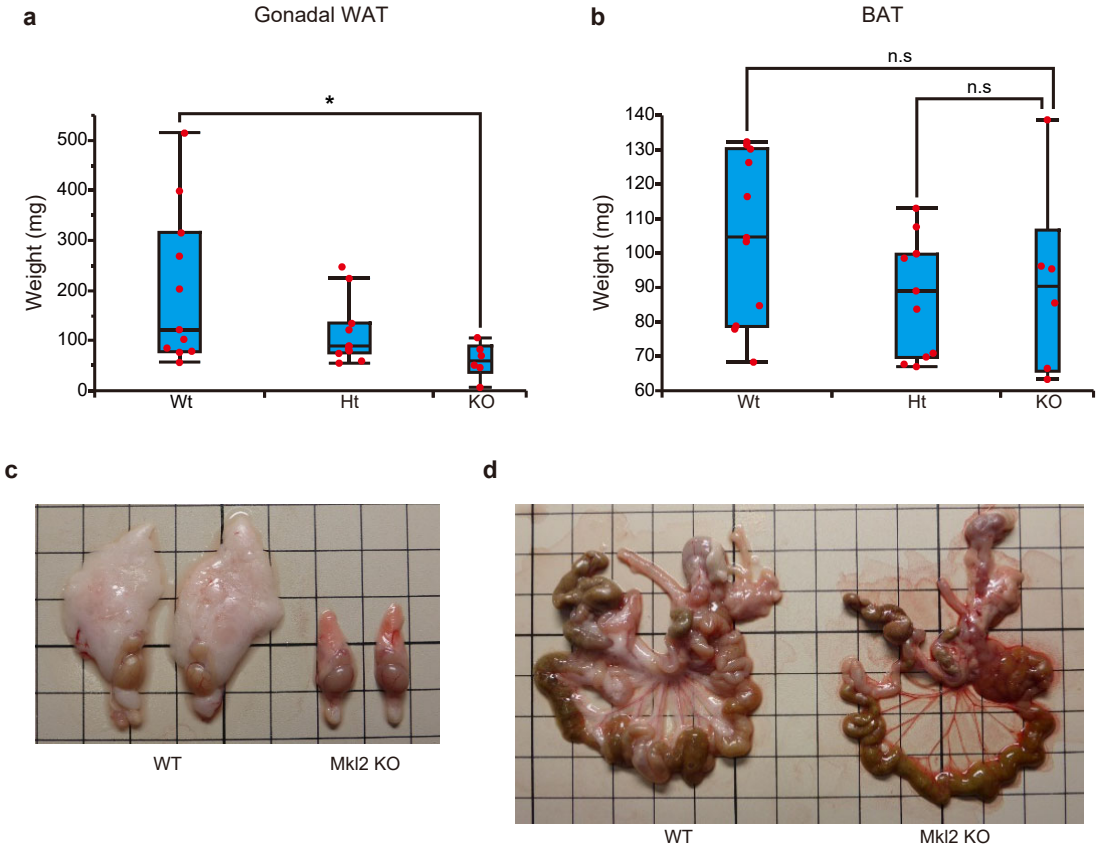

Supplementary Data 2

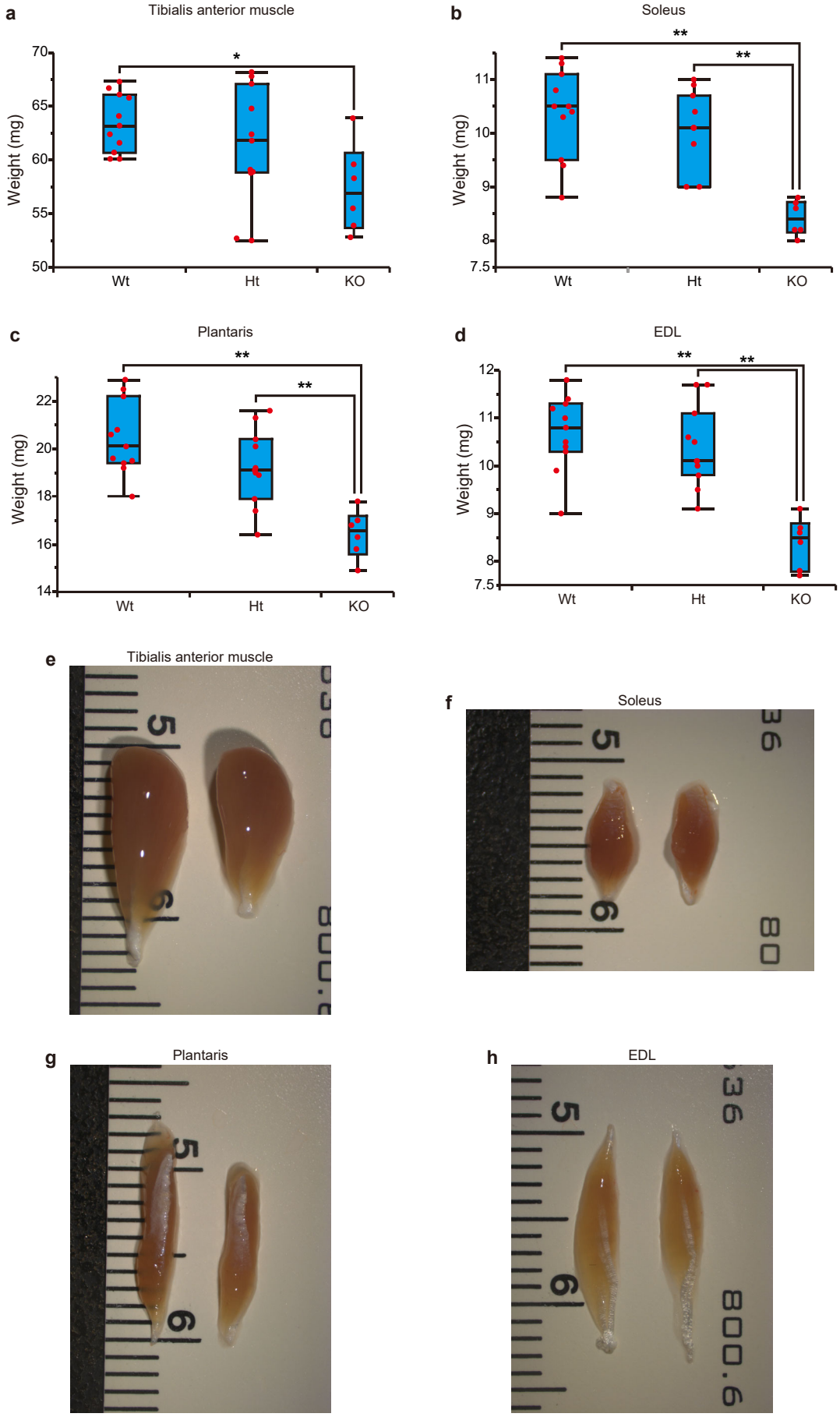

Supplementary Data 3

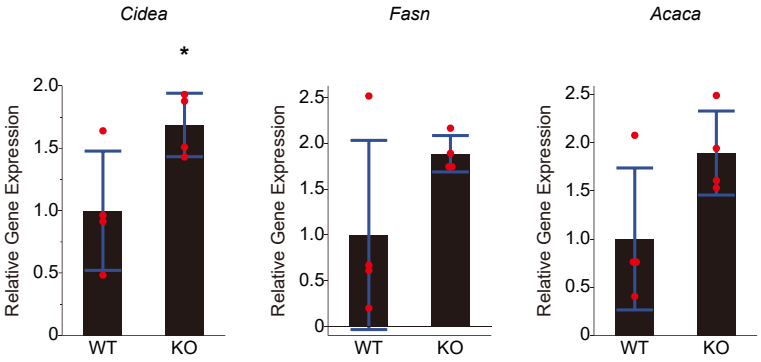

Supplementary Data 4

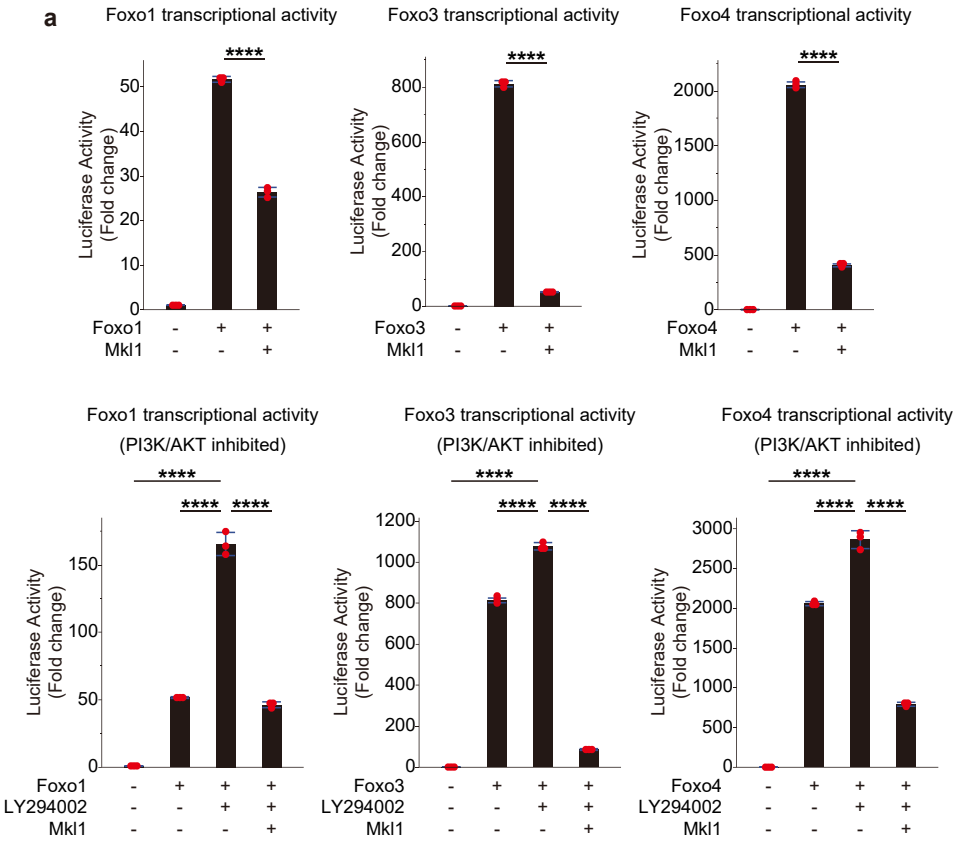

Supplementary Data 5

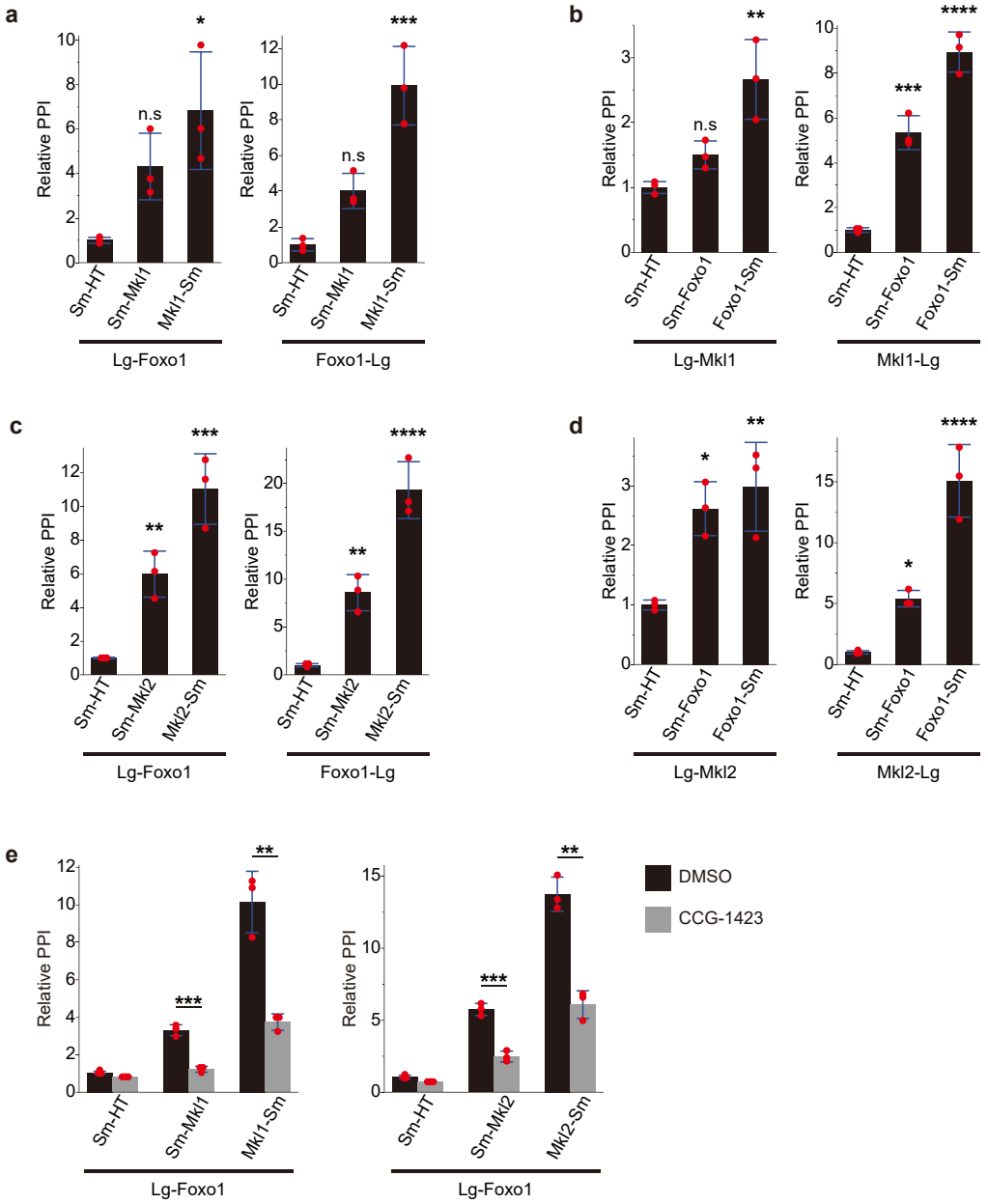

Supplementary Data 6

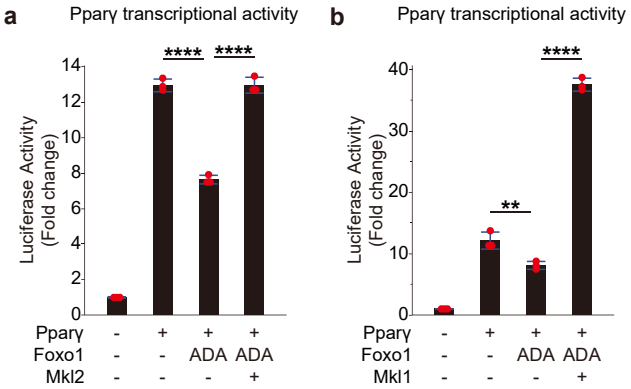

Supplementary Data 7

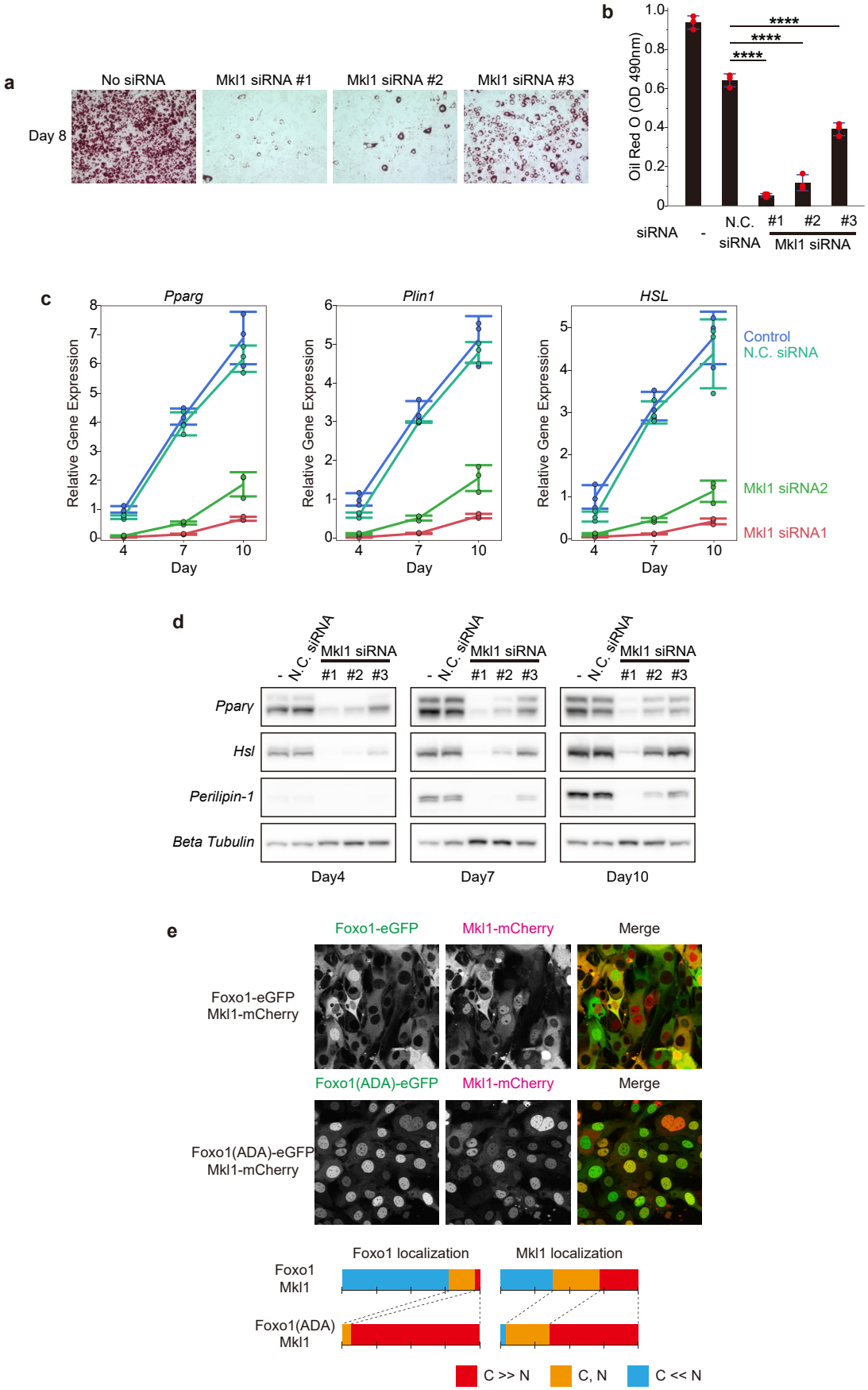

Supplementary Data 8

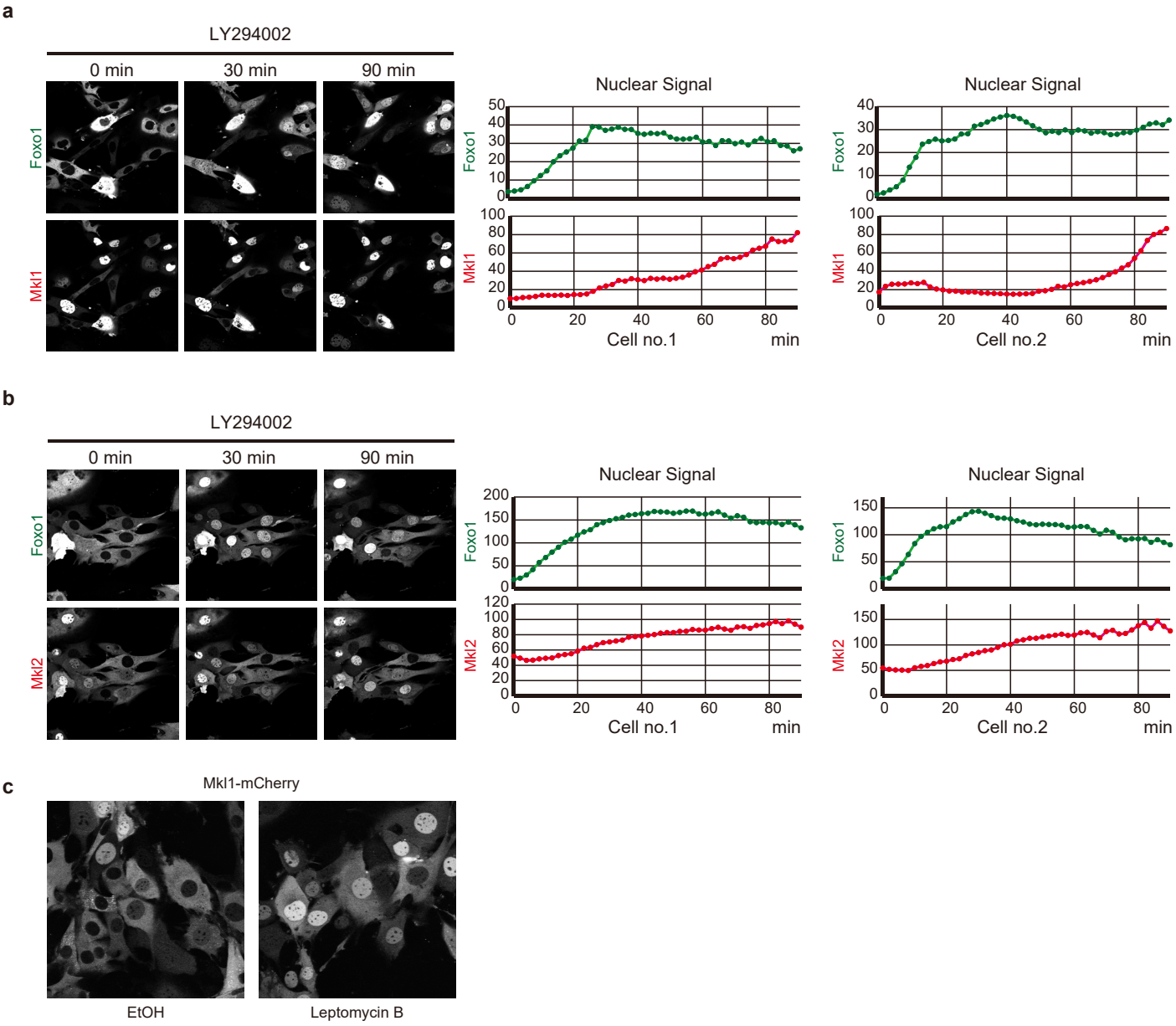

Supplementary Data 9

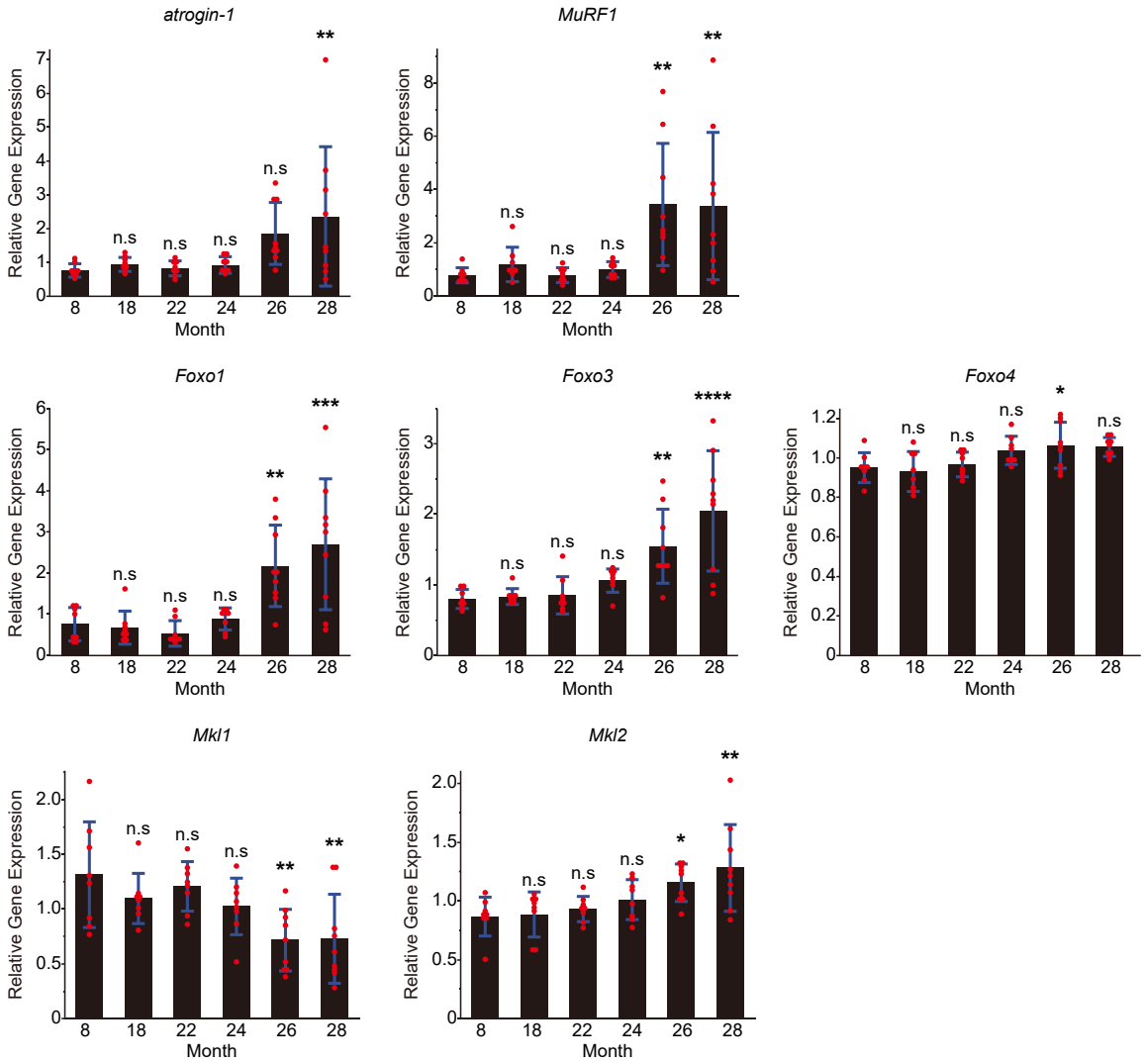

Supplementary Data 10

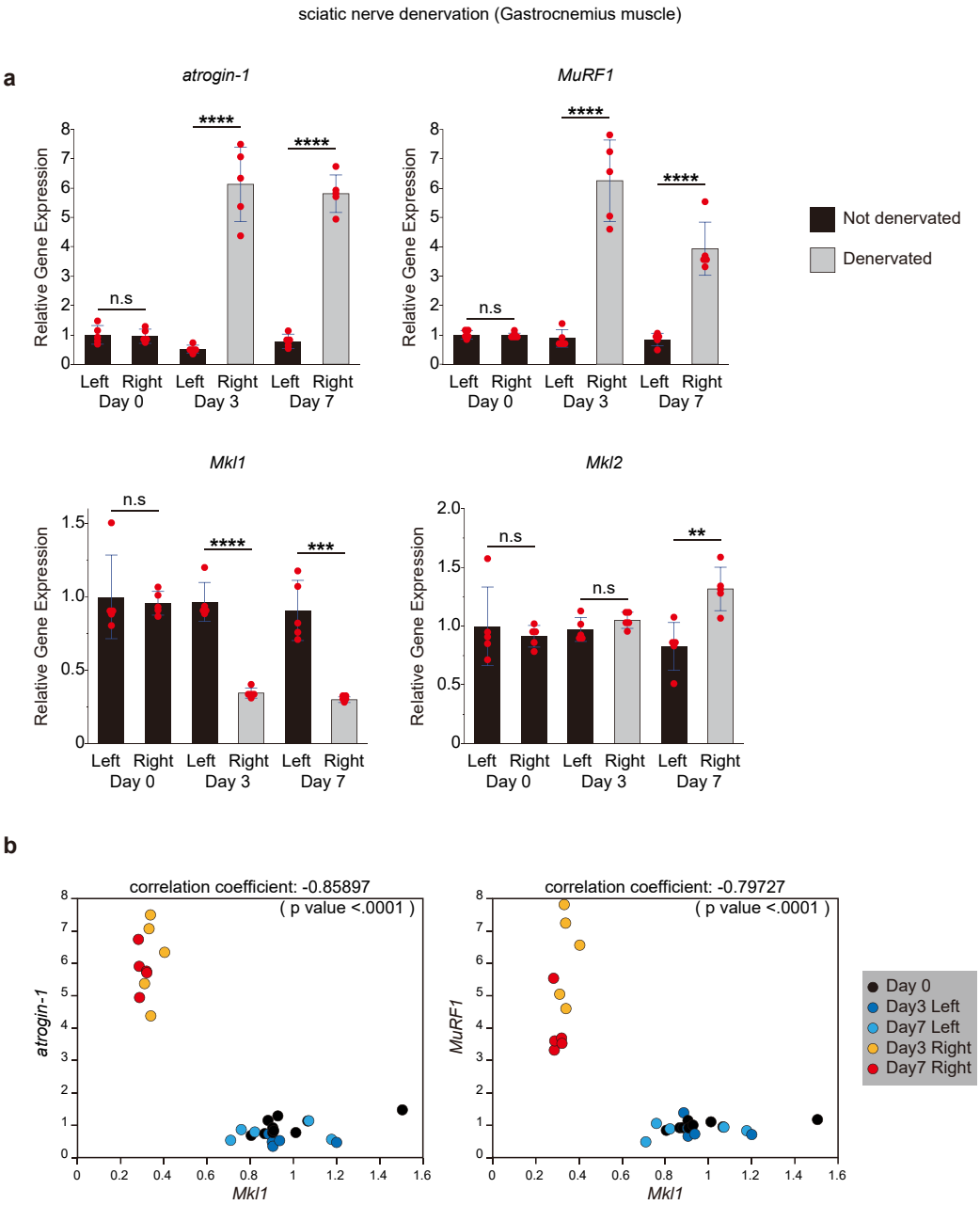

Supplementary Data 11

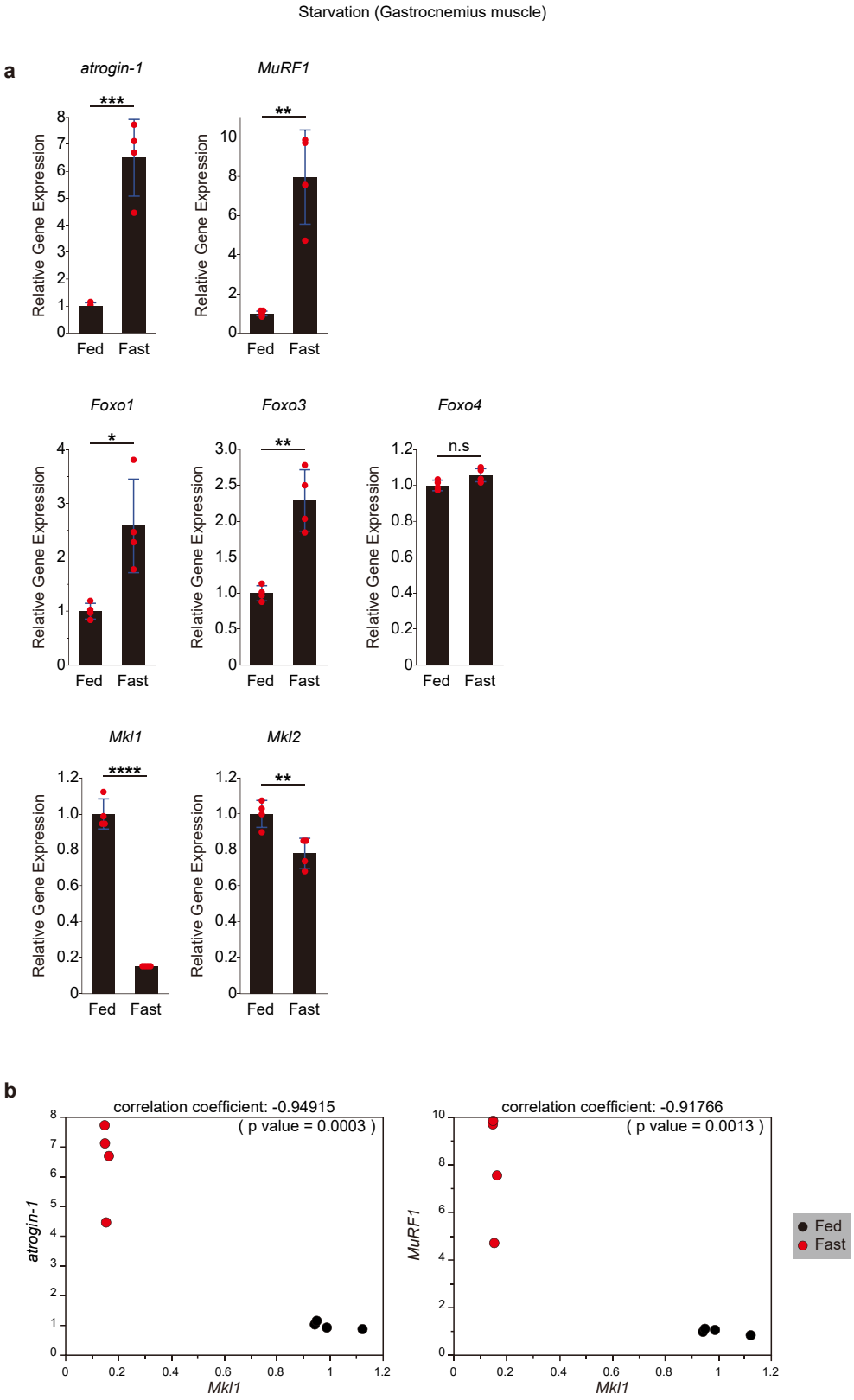

Supplementary Data 12

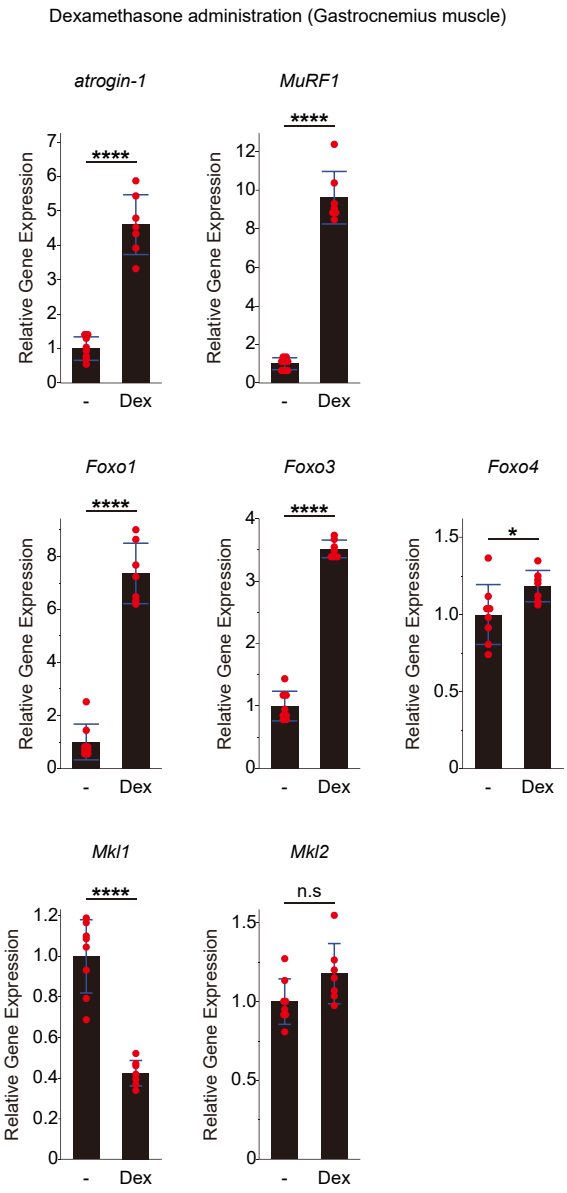

Supplementary Data 13

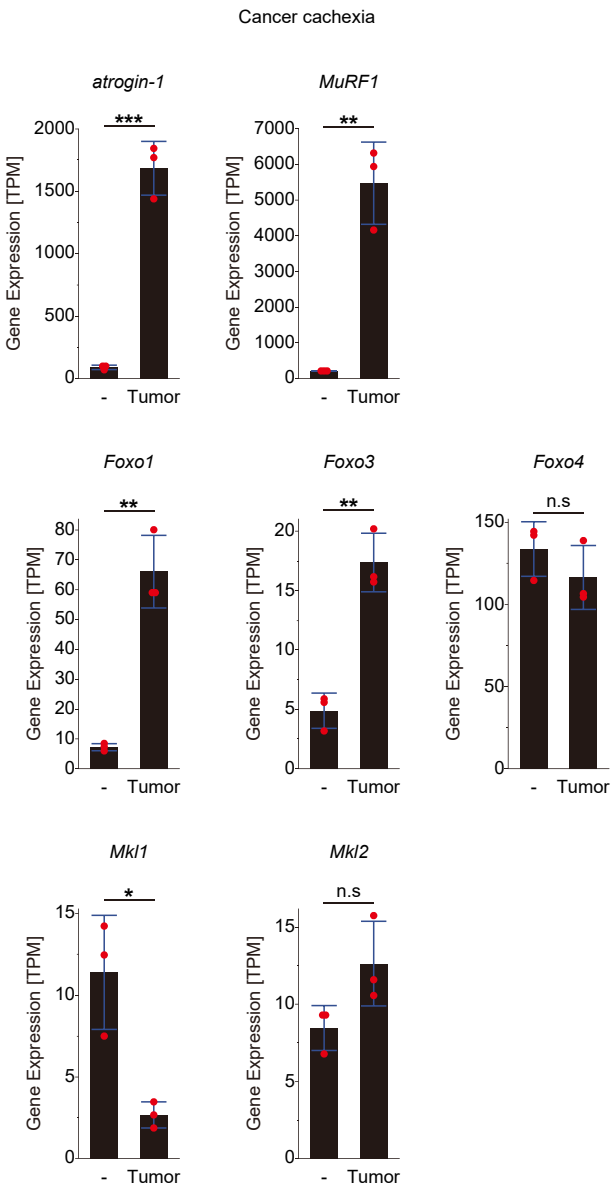

Supplementary Data 14

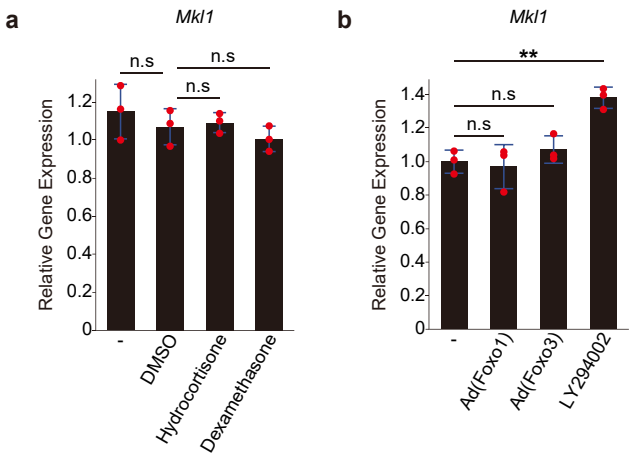

Supplementary Data 15

a

ChIP-qPCR: *atrogin-1*

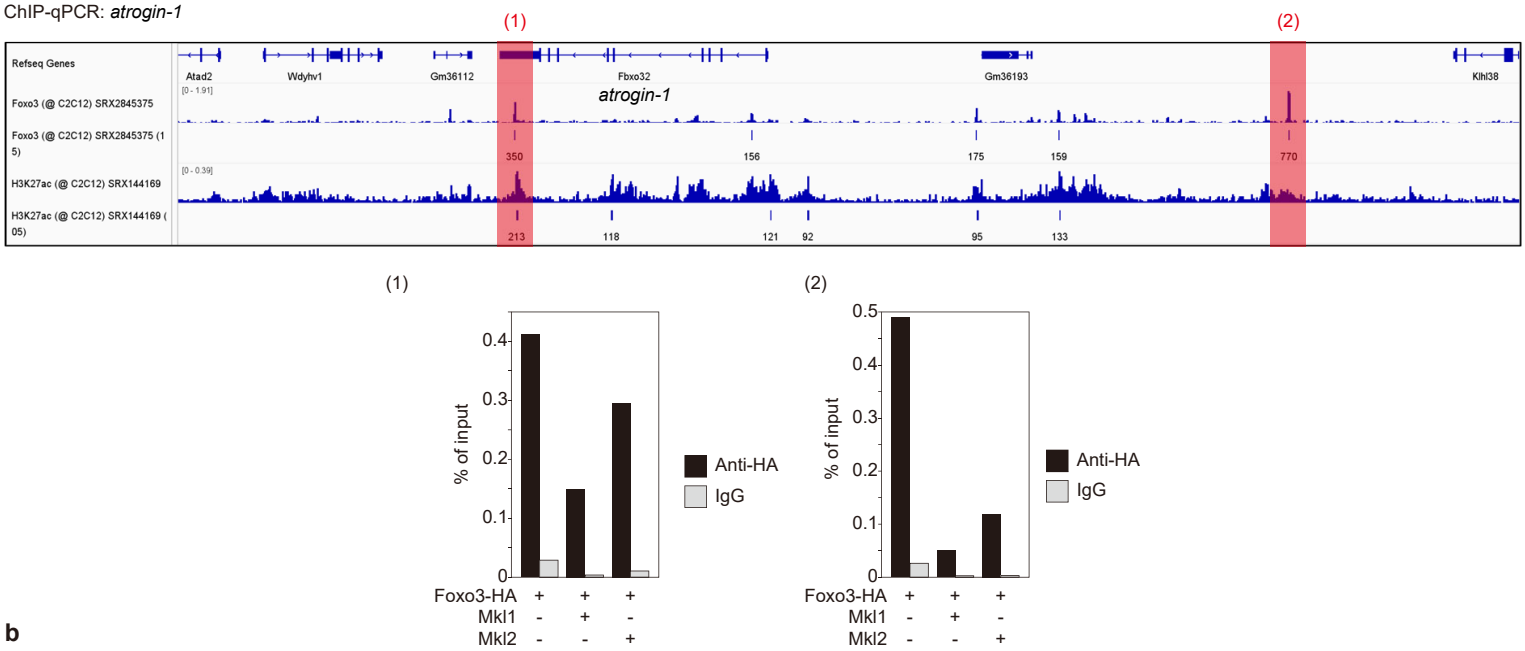

b

ChIP-qPCR: *MuRF1*

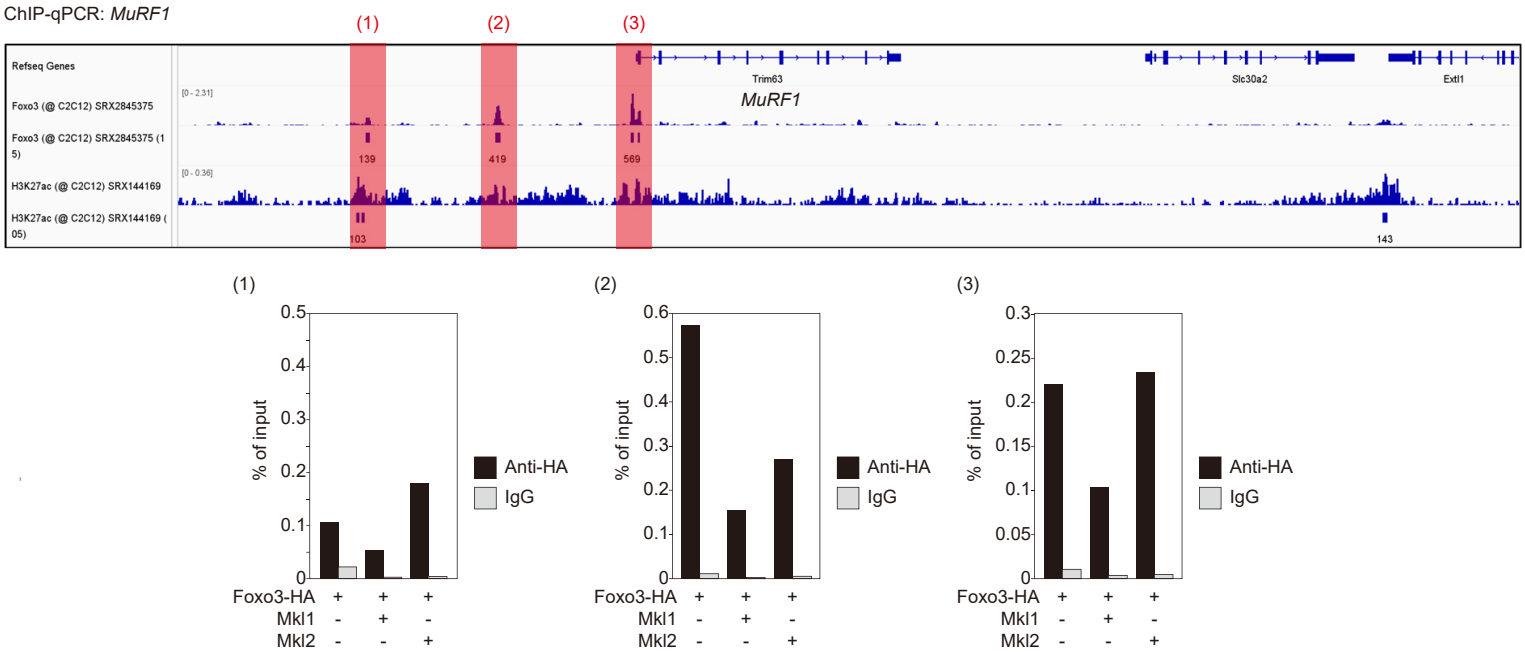

Supplementary Data 16

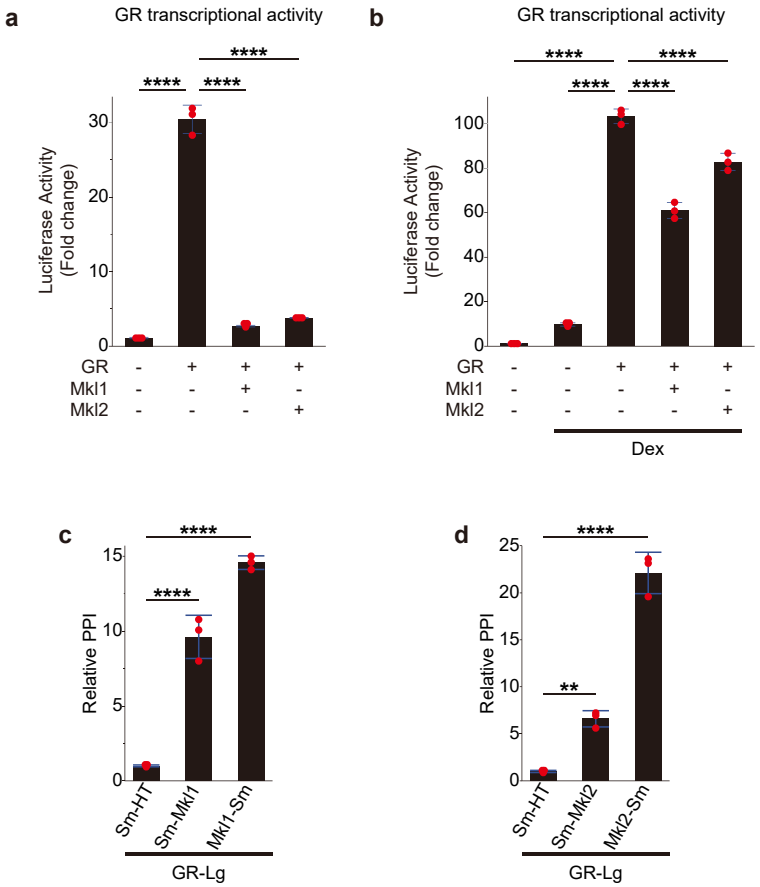

Supplementary Data 17

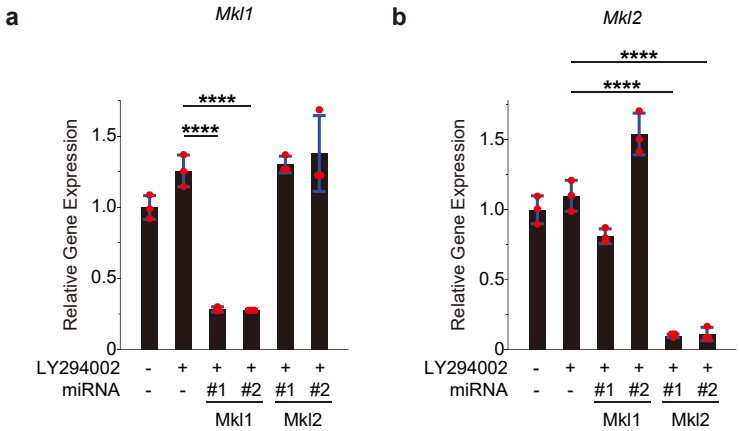

Supplementary Data 18

a

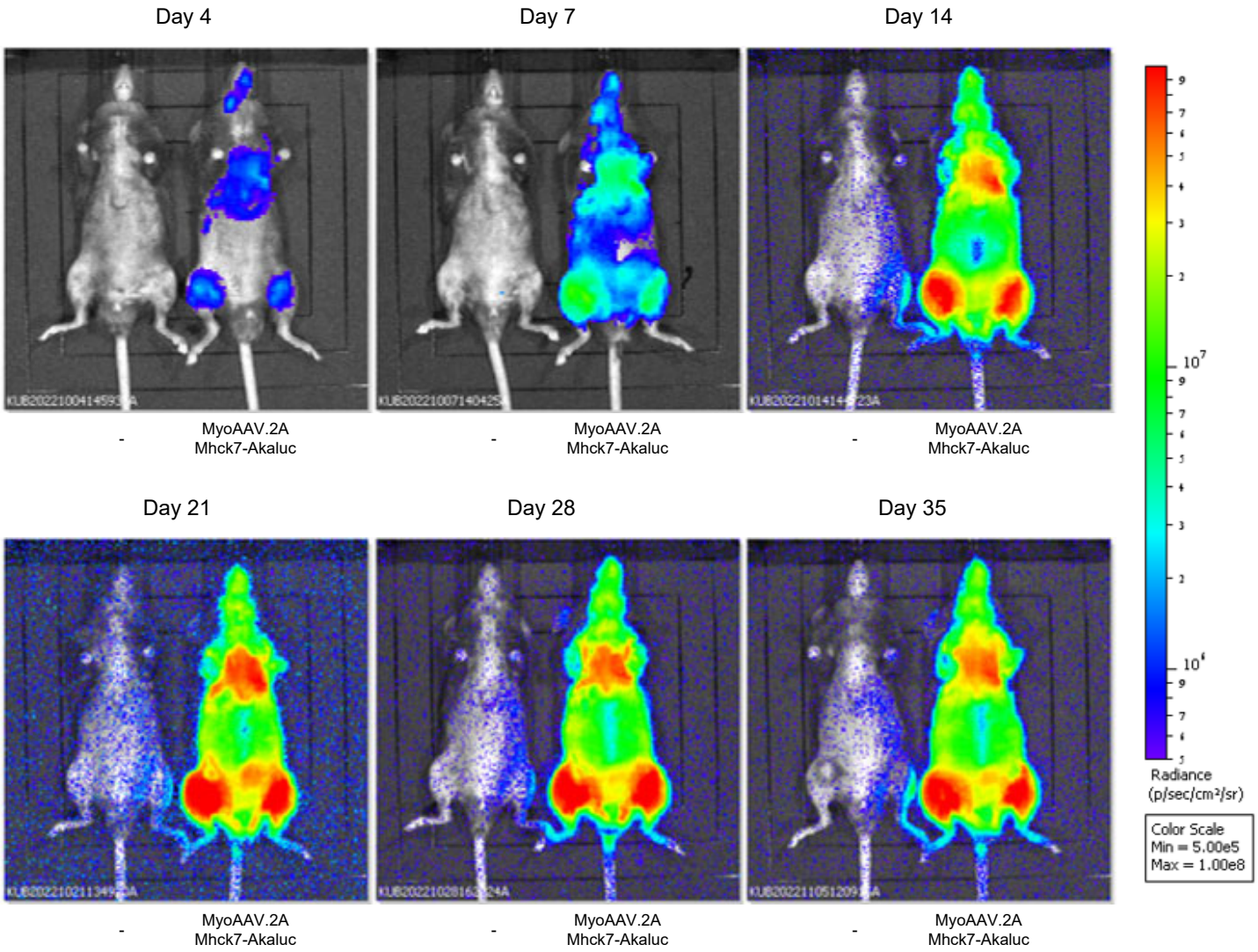

b

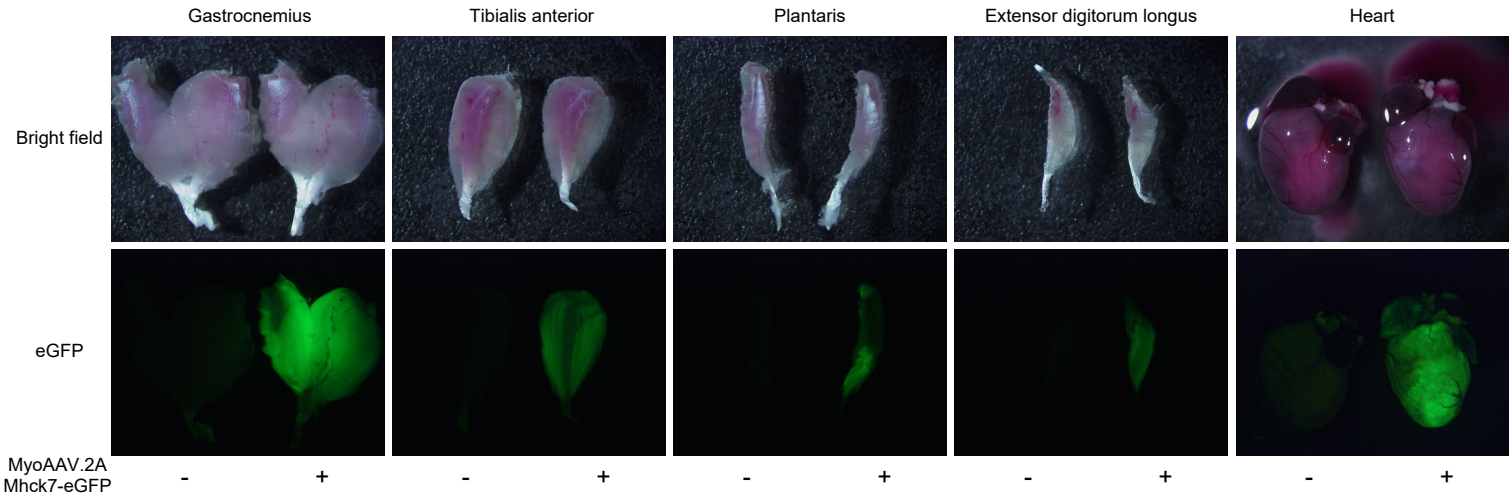

Supplementary Data 19

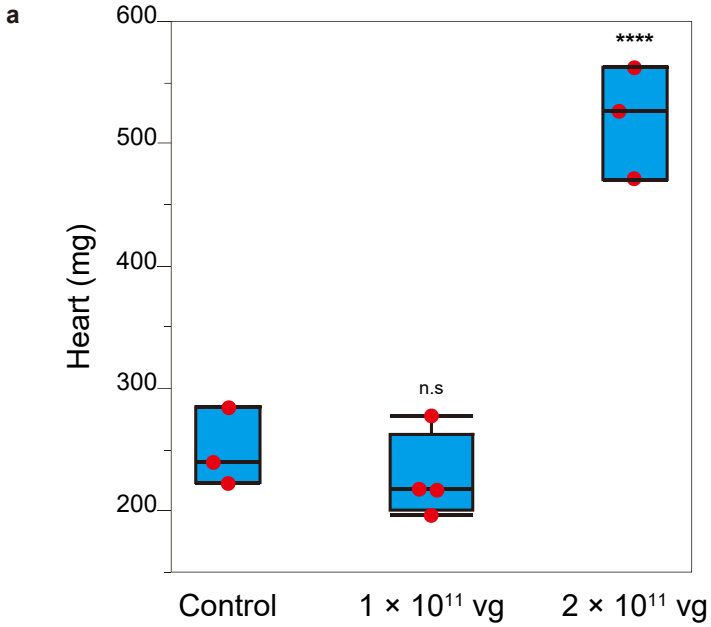

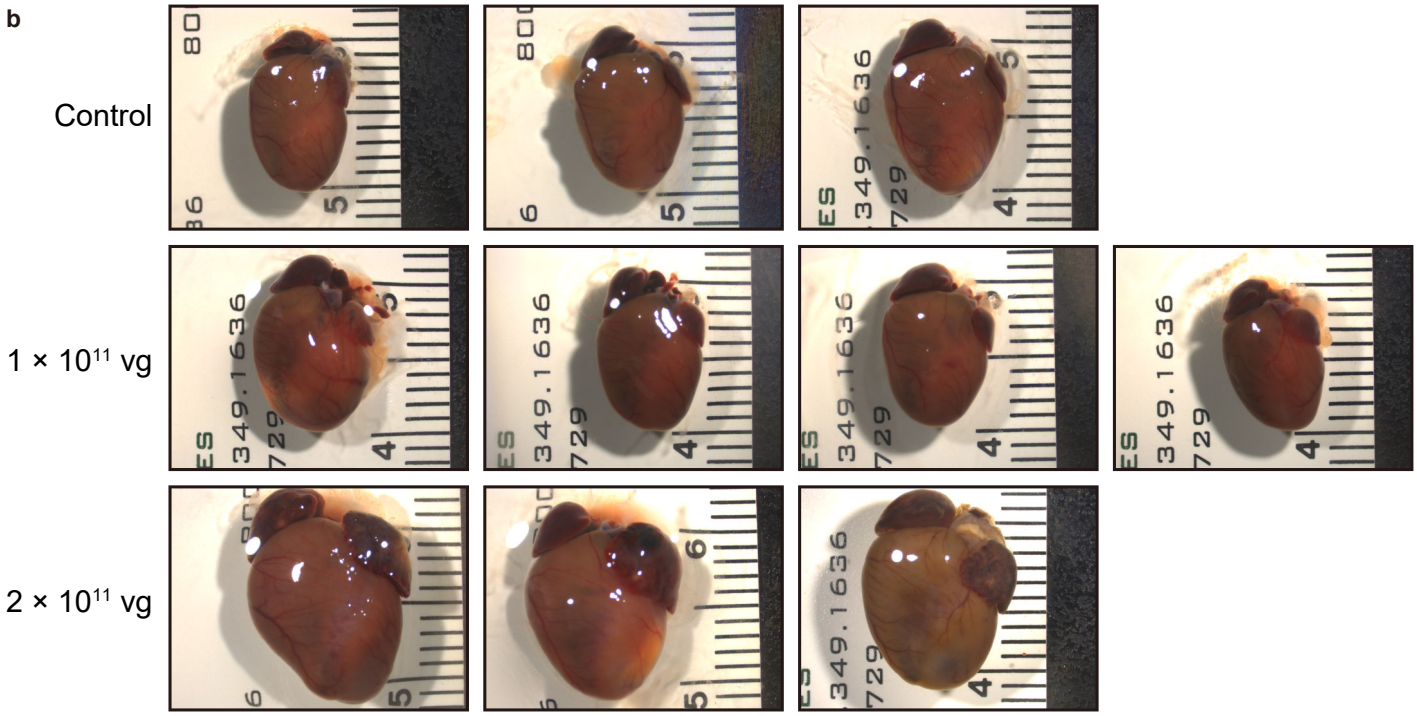

Supplementary Data 20

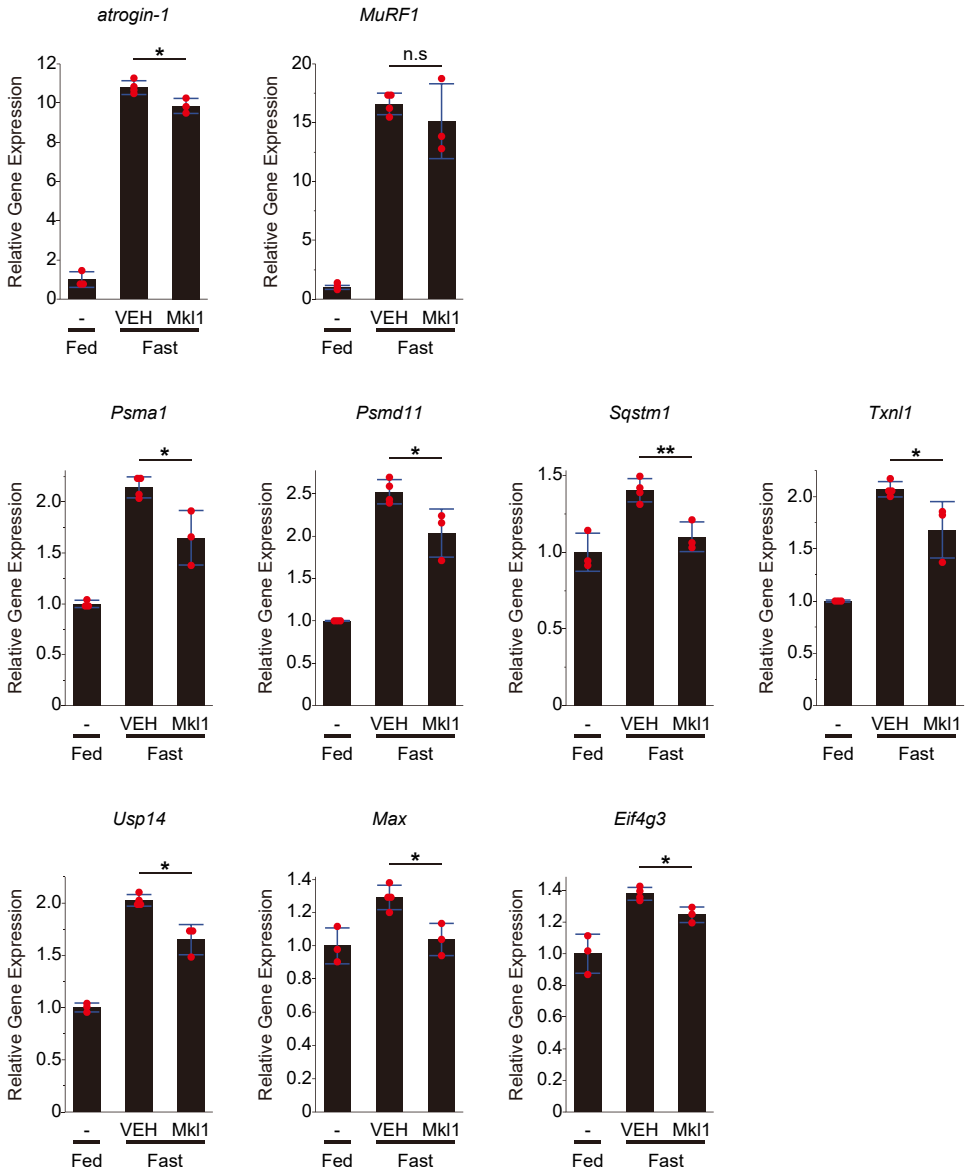
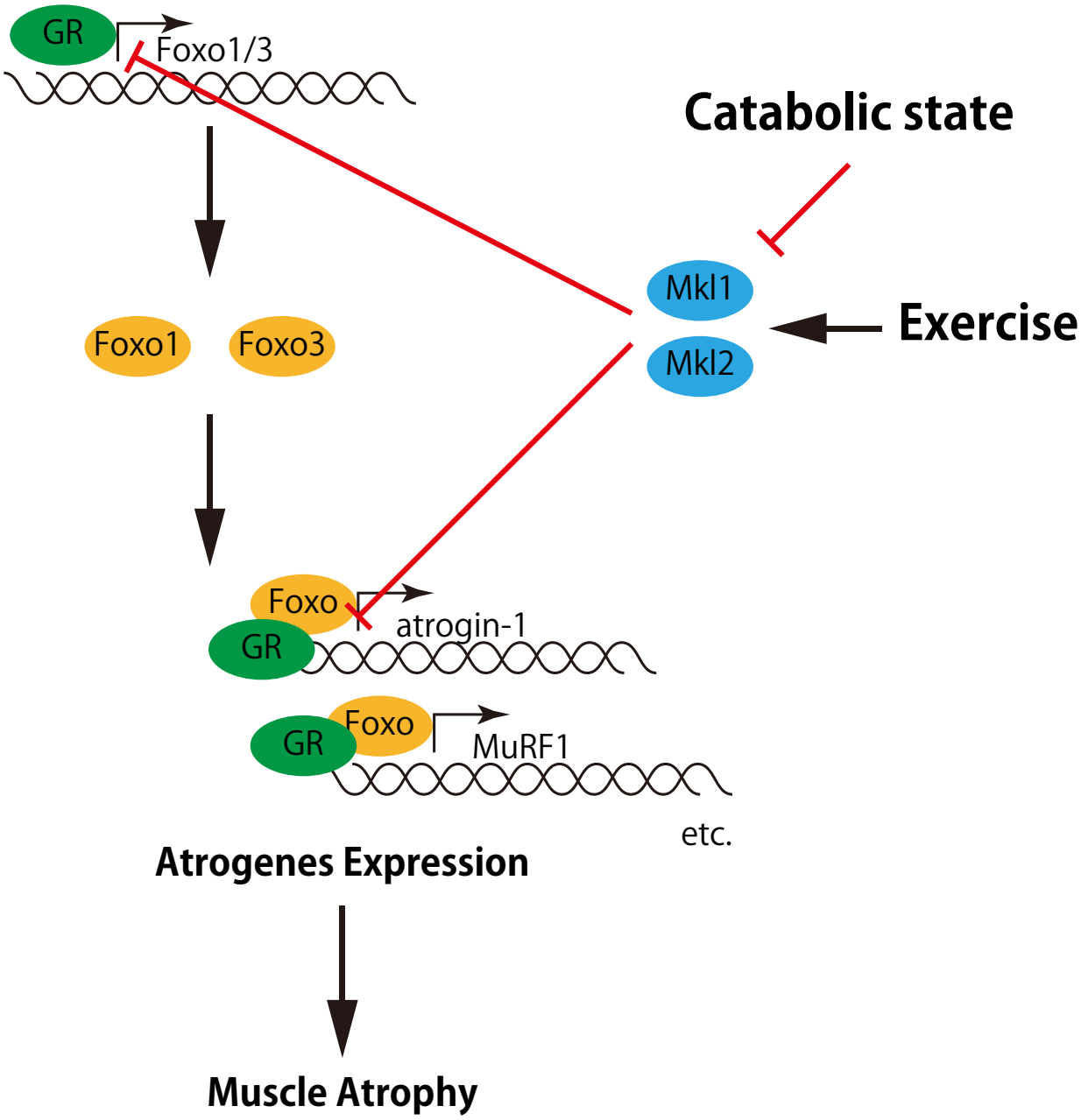
Supplementary Data 21